Coiled double amyloid-like fibrils allosterically catalyze hydrolysis of β-lactam antibiotics

Sisira Mambram Kunnath[1,2#], Elad Arad[1,2,3#], Ran Zalk[1], Itamar Kass[1], Albert Batushansky[1]

*Hanna Rapaport[1,4] and Raz Jelinek[1,2]**

[1] Ilse Katz Institute (IKI) for Nanoscale Science and Technology
Ben Gurion University of the Negev,
Beer Sheva 8410501, Israel

[2] Department of Chemistry
Ben Gurion University of the Negev,
Beer Sheva 8410501, Israel.

[3] Current affiliation: Department of Chemical Engineering,
Columbia University in the City of New York,
New York, NY 10027, USA

[4] Avram and Stella Goldstein-Goren Department of Biotechnology Engineering
Ben Gurion University of the Negev,
Beer Sheva 8410501, Israel.

E-mail: Razj@bgu.ac.il

KEYWORDS: catalytic amyloids; cross-β amyloid fibrils; β-lactam hydrolysis; allosteric mechanisms; coiled fibrils; nucleophilic attack

ABSTRACT

The release of antibiotic compounds into wastewater constitutes a significant and growing health and environmental hazard, particularly contributing to the spread of antibiotic resistant bacterial strains. Here, we demonstrate that amyloid fibrils, consisting of an alternating lysine/phenylalanine β-sheet forming short peptide, catalyze hydrolysis of β-lactam antibiotics, the most prominent family of antibiotic compounds, which is further widespread in wastewater. Peptide variant analysis, molecular dynamics (MD) simulations, and cryogenic electron microscopy (cryo-EM) reveal that the β-lactam molecules dock onto the fibrils' surface via electrostatic interactions with the lysine sidechains. Importantly, catalytic hydrolysis occurs via an allosteric mechanism mediated by a unique coiled double fibril structure in which the anchored β-lactam molecules are embedded within twisted fiber strands, facilitating nucleophilic attacks by the lysine sidechains. Utilization of the catalytic lysine-displaying amyloid fibrils for hydrolytic degradation and removal of β-lactam antibiotics from water was accomplished through display of the fibrils on silica beads placed in a conventional column filtration setup. Amyloid fibrils displaying lysine arrays may furnish a versatile platform for hydrolysis and removal of β-lactam antibiotics in water, underscoring new avenues for addressing the considerable threat of antibiotics water contamination.

Introduction

Since the groundbreaking discovery of penicillin in the last century, small molecule antibiotics have been widely used for preventing or treating bacterial infections in humans and animals[1]. As a consequence, large quantities of antibiotic substances have been released into wastewater, contaminating groundwater, rivers, and the sea[2,3]. Exposure to antibiotics in water bodies

contributes to the spread of antibiotic resistance – among the most significant threats in modern medicine[4,5]. Importantly, there are currently no technologies employed for efficient removal of antibiotic pollutants from water, as methods utilized for elimination of organic pollutants in wastewater, like nanofiltration, ozonation, adsorption, or osmosis are largely ineffective for water-soluble antibiotic treatment[3,6]. Accordingly, there is a pressing need to develop new technologies for deactivation and removal of antibiotic contaminants from water.

Catalytic degradation by biological and biomimetic vehicles may constitute a possible avenue for elimination of antibiotic pollutants in water. Supramolecular peptide assemblies have been shown to catalyze a wide range of biological and chemical reactions[7]. In particular, recent groundbreaking studies have demonstrated that physiological amyloid fibrils exhibit remarkable catalytic properties, including ester hydrolysis, dephosphorylation, lipid degradation, and catecholamine oxidation[8–14]. Cofactor-free catalytic activities of amyloids have been generally ascribed to the creation of amphiphilic pockets, being able to bind substrate molecules and initiate nucleophilic attacks in the active sites[8,15]. We have recently shown that bacterial biofilm-associated cross-α amyloids catalyze hydrolysis of β-lactam antibiotics[16]. This surprising observation may both unveil a novel pathway for antibiotic resistance by amyloid-generating bacteria, as well as illuminate possible new means for achieving β-lactam antibiotic degradation in water. Mechanistically, it was shown that lysine-rich cross-α amyloid fibrils expose primary amines that serve as nucleophiles, enabling effective binding and subsequent hydrolysis of β-lactams[16]. Indeed, other studies have shown that short amyloid-like sequences containing lysine arrays display nucleophilic properties enabling catalysis in low and neutral pH values[17,18].

Synthetic peptides displaying the amphiphilic amino acid pattern Pro-X-(Phe-X)$_5$-Pro, in which the backbone consists of hydrophilic amino acids (X) alternating with hydrophobic phenylalanine residues and prolines at the termini, were shown to adopt β-sheet fibril organization[19]. Specifically, a cationic Pro-Lys-(Phe-Lys)$_5$-Pro variant (denoted PFK), designed for the templating of metallic gold nanofibers[20] and as a drug delivery vehicle[21–24], was shown to adopt β-sheet-based fibrillar structures[21,25]. Importantly, the alternating lysine/phenylalanine sequence of PFK may mimic PSMα3 catalytic activities.

Here, we demonstrate that PFK amyloid fibrils exhibit remarkable catalytic activity towards β-lactam hydrolysis. PFK fibrils, both free-form and displayed on silica beads utilized in conventional water purification settings, were found to catalyze hydrolysis of prominent β-lactam antibiotics, including nitrocefin, penicillin, and amoxicillin. Peptide derivative analysis, complemented by molecular dynamics simulations and cryogenic electron microscopy, point to a unique allosteric catalytic mechanism involving electrostatic interactions of the β-lactam substrates and lysine residues and the formation of coiled fibril structures. This study illuminates amyloid fibrils as a viable platform for antibiotic degradation and removal from water.

Results and discussion

Figure 1 depicts the experimental concept. PFK amyloid fibrils adopt β-sheet organization, displaying the lysine side chains on the fibrils' surface (**Figure 1a**), mimicking the lysine-rich amphiphilic pattern of PSMα3, the functional bacterial amyloid recently shown to catalyze hydrolysis of β-lactams[16]. As shown in Figure 1a, hydrolytic breakup of the four-member β-lactam

ring is catalyzed via interactions with the PFK amyloid fibrils, presumably via nucleophilic attack by the

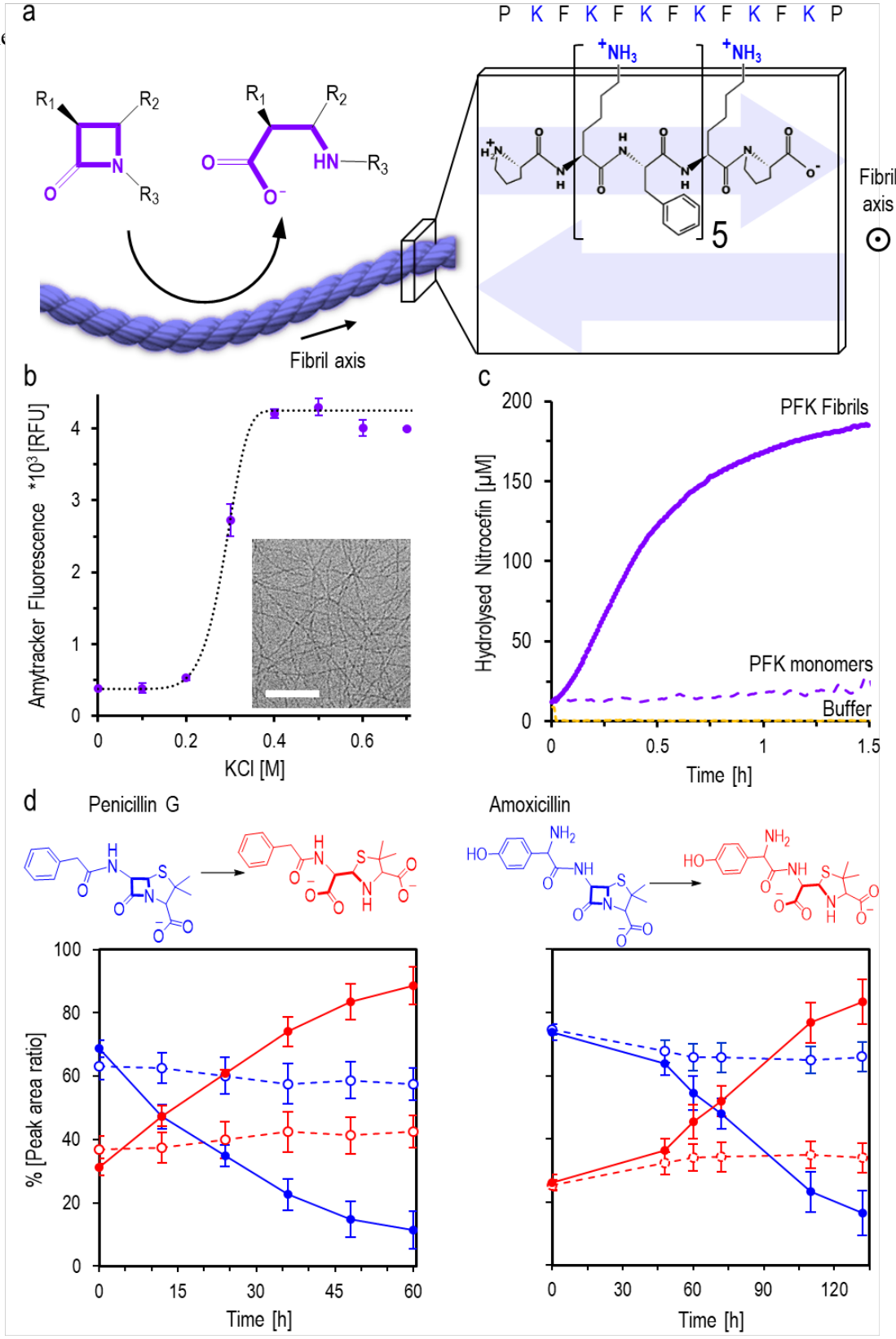

Figure 1. PFK amyloid fibrils catalyze hydrolysis of β-lactam antibiotics. a. The experimental scheme. PFK forms amyloid fibrils comprising an antiparallel cross-β architecture (the PFK sequence is shown on the right, highlighting the surface-displayed nucleophilic lysine sidechains). The fibrils' surface induces catalysis of β-lactam hydrolytic ring. **b.** Fluorescence emission of PFK (0.2 mM) incubated with the amyloid-sensitive fluorescence dye Amytracker-680 (Ex= 550 nm, Em= 650 nm), as a function of KCl concentration. The inset shows a representative cryo-TEM image of PFK amyloid fibrils upon incubation with 0.2 M KCl. **c.** Nitrocefin hydrolysis recorded upon incubation with PFK fibrils (PFK concentration 0.2 mM; KCl 0.2 M), and PFK monomers (no KCl added). The concentration of hydrolyzed nitrocefin was determined by measuring the absorbance at 480 nm in the reaction mixture. **d.** PFK amyloid fibril-catalyzed hydrolysis of penicillin and amoxicillin. The substrate molecules were incubated with PFK at pH=7.4 and the relative abundance of the reactants and hydrolysis products (shown in the chemical reaction schemes) were determined by LC-MS. Solid blue and red curves represent the reactant and product, respectively, following incubation with the PFK amyloid fibrils, while the broken curves correspond to the control experiments (no PFK fibrils added).

The fluorescence emission experiment depicted in **Figure 1b** confirms that PFK adopts fibril organization. Specifically, Figure 1b presents the fluorescence emission of the amyloid-reporting dye Amytracker-680[26] upon its incubation with PFK (0.2 mM) dissolved in aqueous solutions comprising different KCl concentrations. PFK folding to β-sheet-based fibril formation is highly sensitive to the ionic strength, which interferes with the electrostatic repulsion between the positively charge lysine residues[27]. Specifically, shielding of the electrostatic repulsion permits stacking of the peptide-chains in a juxtaposed antiparallel cross-β conformation (Figure 1a) and consequent fibril formation[21,25]. Figure 1b demonstrates that above a KCl concentration of approximately 0.2 M, fluorescence of the dye rapidly increased, indicating fibrillation of the PFK peptide[16,26]. Second derivative analysis of the fluorescence curve in Figure 1b confirms that 0.2 M

KCl is the threshold concentration for fibril formation (Figure S1). The structure transformation of PFK at 0.2M KCl is further supported by circular dichroism (CD) spectral data (Figure S2) indicating a polyproline type II - β-sheet transformation, and Fourier transform infrared (FTIR) spectroscopy (Figure S3). The TEM image in the inset in Figure 1b shows the abundant PFK amyloid-like fibrils assembled. It should be noted that above a critical assembly concentration of 2 mM, PFK displays a propensity to fibrillate even without salt present, due to the amphiphilic nature of the peptide[25,28].

The thrust of this study is the catalytic properties of PFK amyloid fibrils towards β-lactam hydrolysis. Indeed, **Figure 1c** demonstrates that PFK amyloid fibrils catalyze hydrolysis of nitrocefin, a widely studied β-lactam surrogate[29]. Nitrocefin undergoes a yellow to red transformation due to hydrolysis of the amide unit in the β-lactam ring. The colorimetric changes can be readily monitored by visible absorbance spectroscopy, and corresponding concentrations of the hydrolyzed reaction product can be determined through calibration. Figure 1c portrays a pronounced increase in the absorbance of hydrolyzed nitrocefin in the presence of PFK amyloid fibrils, reflecting their catalytic activity (solid blue curve). In contrast, monomeric PFK (e.g., the peptide dissolved in a buffered solution not containing KCl) did not induce nitrocefin hydrolysis (broken blue curve in Figure 1c).

The experimental data in **Figure 1d** reveal that PFK fibrils catalyze hydrolysis of other β-lactam antibiotics, specifically penicillin and amoxycillin, ubiquitous clinical β-lactam antibiotics[30]. In the experiments, the relative concentrations of β-lactam substrates and hydrolyzed reaction products were determined by liquid-chromatography-mass spectrometry (LC-MS)[30]. Notably, for both penicillin and amoxycillin, incubation with PFK amyloid fibrils significantly accelerated the

hydrolysis reactions (i.e. decrease of substrate concentrations, blue curves, and increase in hydrolyzed products, red curves in Figure 1d). For example, in the presence of PFK fibrils the relative abundance of penicillin decreased from 69% to 11% after 60 hours of co-incubation, while the percentage values in the case of amoxycillin were 74% initially, 17% after incubation with PFK amyloid fibrils (chromatograms are presented in Figures S4 and S5). Note that some hydrolyzed products were observed prior to addition of PFK amyloid fibrils - ascribed to spontaneous hydrolysis of the antibiotics, typical for varied β-lactams[31]**.** However, hydrolysis of the control samples (β-lactam substrates in buffer, without the presence of PFK fibrils) was significantly less pronounced in comparison with fibril-incubated samples (Figure 1d, broken curves).

The catalytic activity induced by PFK amyloid fibrils, i.e. initial hydrolysis reaction rates extracted from the absorbance curves versus initial substrate concentrations, is presented in **Figure 2** (KCl concentrations were 0.2 M in all samples, assuring fibril formation). Importantly, the experimental data can be fitted according to two distinct catalytic models (fitted purple and orange curves, Figure 2). If we consider all datapoints, a sigmoidal curve is apparent upon fitting to the Hill equation (purple curve in Figure 2), generally employed for analysis of interactions between ligands and biological macromolecules[32]. The sigmoidal curve indicated an allosteric, cooperative behavior of the amyloid fibril catalyst and nitrocefin substrates, which is also manifested in the Hill coefficient value of 7[13,33]. Indeed, sigmoidal-type activities are the hallmark of allosteric enzymes such as proteases[34]. Allosteric behavior, however, has not been previously reported for catalytic peptides**.** Interestingly, if one considers only the lower nitrocefin concentration datapoints (i.e., nitrocefin concentrations < 300 μM, Figure 2), the experimental data can be fitted to a Michaelis-Menten-like catalytic model (Hill coefficient 1.2, parameter table in Figure 2).

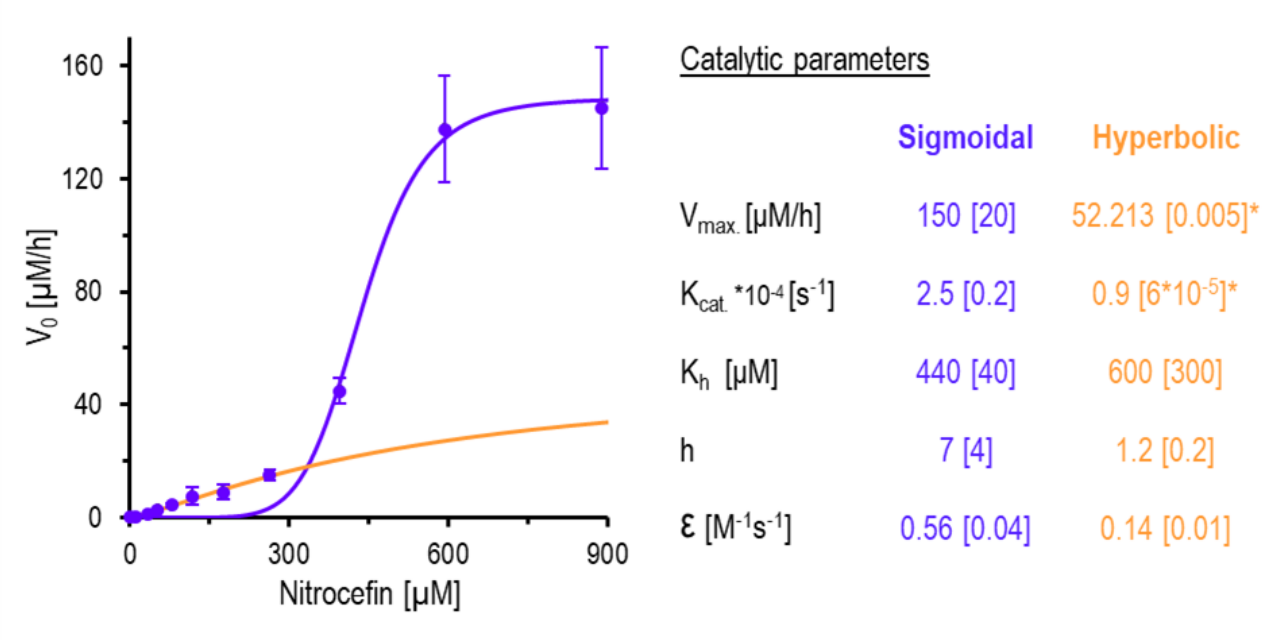

Figure 2: Catalytic activity of PFK amyloid fibrils in nitrocefin hydrolysis. The datapoints represent the measured initial rates (V_0) extracted from the absorbance curves accounting for nitrocefin hydrolysis. The sigmoidal purple curve corresponds to fitting of the entire data set to the Hill equation. The orange line corresponds to fitting of only the low nitrocefin concentrations (< 300 µM), showing quasi-hyperbolic pattern. The catalytic parameters extracted from the two fittings are presented on the right. The measurements were repeated five times in independent experiments (n=5) and the V_0 values are presented as average ± SEM. The catalytic parameters were derived from nonlinear regression of the Hill equation to the average values, where the errors are the confidence-intervals of the fitting.

The catalytic parameters extracted from the V_0 curves in Figure 2 shed light on the two nitrocefin hydrolysis pathway models. While the binding constants (K_h) are at the same order of magnitude, K_h calculated in the case of the allosteric (sigmoidal) model is lower, indicating stronger binding of the nitrocefin substrate molecule to the PFK amyloid fibrils. Furthermore, the maximal reaction rates, V_{max}, yield a significantly higher turnover constant (K_{cat}) for the allosteric behavior,

accounting for faster release of the hydrolyzed nitrocefin reaction product. Overall, the catalytic efficiency (K_{cat}/K_h) according to the allosteric catalytic model is approximately four times more pronounced than the MM-like model (manifested in low nitrocefin concentrations), indicating that the structural rearrangement of the nitrocefin substrate/PFK fibril complex in higher nitrocefin concentrations significantly enhanced the catalytic efficiency.

We measured the effect of an anti β-lactamase antibody upon PFK fibril-induced nitrocefin hydrolysis (**Figure 3)**. This experiment was designed to assess whether the PFK amyloid fibril-induced β-lactam hydrolysis resembles enzymatic (lactamase) pathways. To prevent salt effects which might modulate antibody structure or interactions with the peptide, PFK fibrils were prepared without KCl at a concentration above the fibrillation threshold [i.e., prepared at a concentration of 5 mM, which is above the critical aggregation concentration (CAC) of PFK[28]], and subsequently placed in the reaction mixture. Indeed, the visible absorbance curves in **Figure 3a** demonstrate that the anti-β-lactamase antibody effectively inhibited the catalytic activity of the PFK amyloid fibrils.

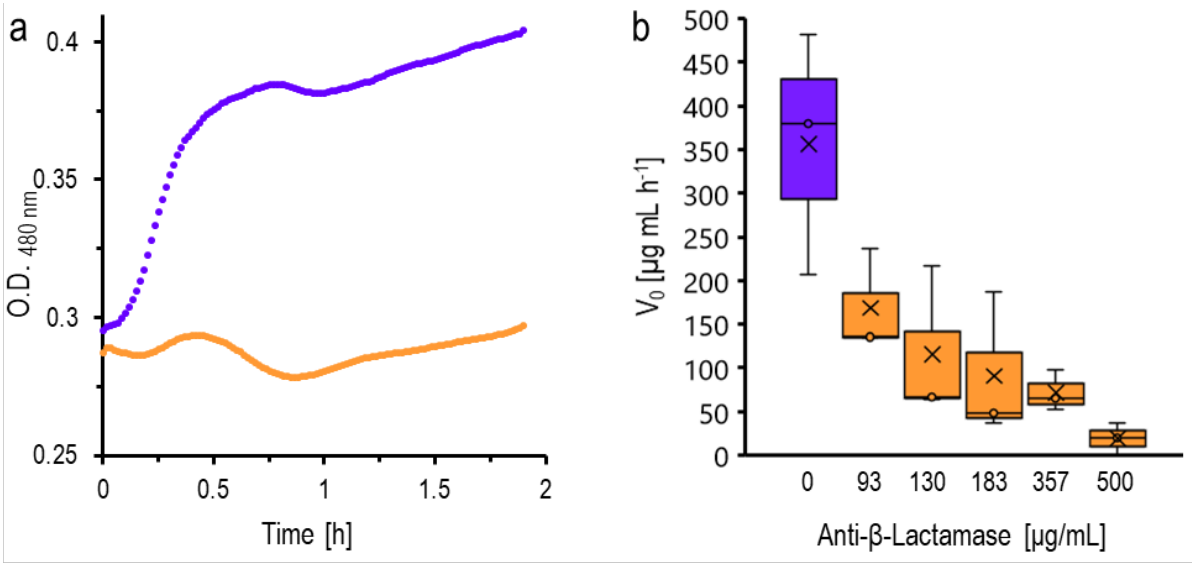

Figure 3. Effect of an anti-β-lactamase antibody on PFK amyloid fibrils'-induced nitrocefin hydrolysis. a. Nitrocefin degradation in the presence of PFK fibrils with (orange curve) and without (purple curve) anti-β-lactamase antibody added. **b.** Initial nitrocefin hydrolysis reaction rates in the presence of PFK amyloid fibril (2 mM), upon addition of different concentrations of anti-β-lactamase antibody. The purple rectangle represents the sample without antibodies added.

The inhibitory effect of the anti-β-lactamase antibody is also manifested in **Figure 3b,** depicting the initial reaction rate (V_0, calculated from the visible absorbance curves) vs antibody concentrations. Specifically, while without antibody co-incubation PFK amyloid fibrils exhibited an initial reaction rate of approximately 350 µg/µL*h, addition of just 2.9 µM antibody, almost three orders of magnitude lower than the PFK concentration, reduced V_0 almost by half, and higher antibody concentrations further inhibited PFK amyloid fibril catalysis (Figure 3b). Overall, the anti-β-lactamase antibody experiments in Figure 3 suggest that the PFK amyloid fibrils surface may exhibit structural features that mimic β-lactamase active sites.

To further probe the key structural features affecting PFK fibrils-catalyzed β-lactam hydrolysis, we investigated the structural and catalytic properties of several PFK-derived peptide variants, exhibiting different fiber morphologies, surface charges, and nucleophilic properties (**Figure 4**). **Figure 4a** presents the sequences tested, highlighting the cationic and anionic residues (blue and red, respectively), formal charges (at neutral pH), and surface charges of the peptide assemblies (i.e., ζ-potential). **Figure 4b** presents cryo-TEM images of the aggregates formed by the different variants. Notably, only variants consisting of alternating cationic/non-polar amino acid sequences (PFR, PFDK,) adopted fibril organization. The formation of organized β-sheet amyloid fibrils for these variants was further confirmed by circular dichroism (CD) and Fourier transform infrared (FTIR) experiments (Figures S6). Altogether, the variant assembly data are consistent with previous studies linking amphiphilic sequence patterns with β-sheet folding and fibril formation[28,35,36].

Figure 4c presents a comparative analysis of PFK and PFR fibrils' catalytic properties towards nitrocefin hydrolysis. Specifically, PFS, PFD, PFDK and ScFK did not exhibit β-lactam hydrolytic activity (V_0 values close to zero for all these variants) likely accounting for the absence of organized fibril structure (for ScFK), or lack of / lower abundance of lysine sidechains serving as nucleophilic sites (in the case of PFS, PFD, and PFDK). Furthermore, PFS, PFD, and PFDK fibrils are anionic or zwitterionic (Figure 4a), thereby exhibiting electrostatic repulsion to the negatively charged nitrocefin molecules (at physiological pH).

a

Peptide	Sequence													F.C.	ζ [mV]
PFK	P	K	F	K	F	K	F	K	F	K	F	K	P	+6	10±3
PFR	P	R	F	R	F	R	F	R	F	R	F	R	P	+6	23±1
PFS	P	S	F	S	F	S	F	S	F	S	F	S	P	0	-19±1
PFD	P	D	F	D	F	D	F	D	F	D	F	D	P	-6	-32±3
PFDK	P	D	F	K	F	D	F	K	F	D	F	K	P	0	-1.1±0.5
ScFK.	K	F	F	P	K	K	P	F	K	F	F	K	K	+6	12±2

b

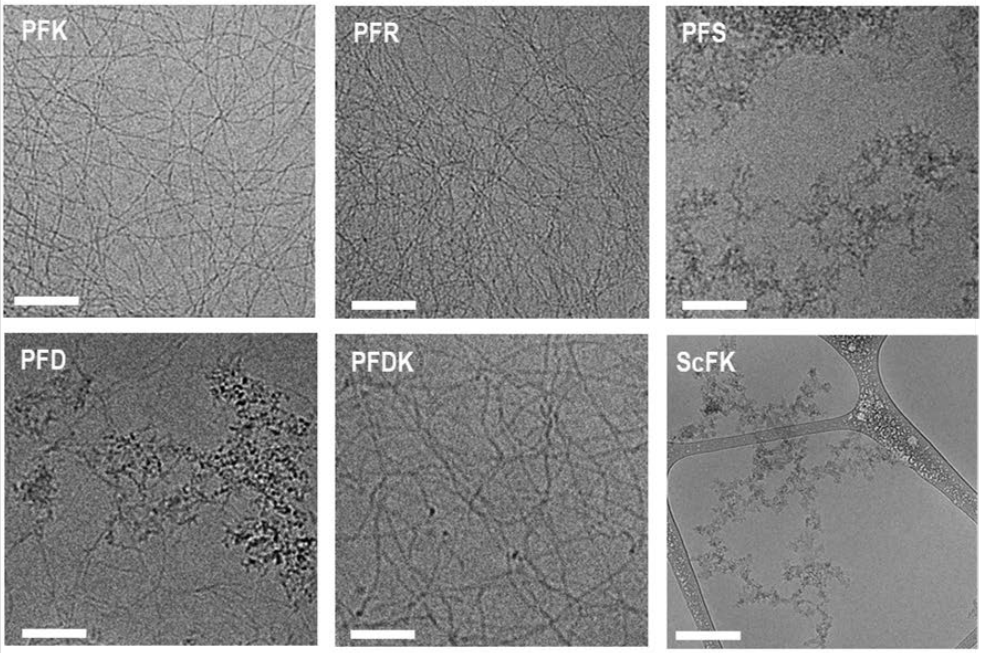

c

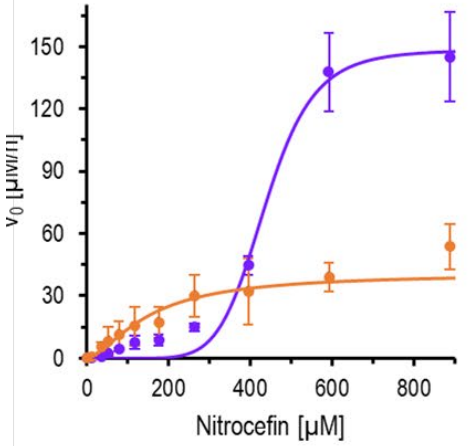

d

	PFK	PFR
$V_{max.}$ [μM/h]	150 [20]	41 [9]
$K_{cat.}$ *10^{-3}[s^{-1}]	2.5 [0.2]	0.05 [0.01]
K_h [μM]	440 [40]	160 [70]
h	7 [4]	1.6 [0.7]
ε [M^{-1}s^{-1}]	0.56 [0.04]	0.43 [0.09]

Figure 4. Structural and catalytic properties of PFK variants. **a.** Sequences of the peptide variants tested. The hydrophilic residues are marked in red, blue, and green, representing anionic, cationic and uncharged residues, respectively. The formal peptide charges and ζ-potentials of the peptide assemblies (prepared at 0.2 mM, Hepes buffer 50 mM, pH 7.4 supplemented with 0.2 M KCl) are also indicated. **b.** Cryo-TEM images of the peptide assemblies (0.2 mM peptide concentrations, dissolved in Hepes 50 mM pH 7.4, KCl 0.2 M. Bars correspond to 200 nm. **c.** Initial nitrocefin-hydrolysis reaction rates calculated for PFK fibrils (purple curve) and PFR fibrils (orange curve). V_0 of the other variants are presented in Figure S7. Peptide concentrations 0.2 mM, dissolved in Hepes 50 mM at pH 7.4, KCl 0.2 M. The values are presented as an average ± SEM, n=5. The catalytic parameters derived from the fitting of the V_0 curves for PFK and PFR to the Hill equation. The values in the brackets represent the confidence intervals.

Figure 4c indicates that PFR also catalyzes nitrocefin hydrolysis, albeit variability in both catalytic efficiencies and mechanisms are apparent, illuminating key parameters accounting for the catalytic activity of PFK amyloid fibrils. Like PFK, PFR also formed cationic fibrils but displayed a significantly different catalytic profile. Specifically, PFR fibrils gave rise to a hyperbolic catalytic curve, reflecting a MM-like mechanism (Hill coefficient equals 1.6), less pronounced substrate binding (K_h=160 μM), and lower maximal reaction rate (V_{max} = 41 μM/h), primarily linked to the low turnover constant (K_{cat} of 0.05 s^{-1}) (Figure 4d). The low K_h and K_{cat} values account for relatively high stability of the fibril-substrate complex, which constitutes a barrier to progression of the hydrolysis reaction and overall lower catalytic efficiency. Overall, the comparative catalytic analysis in Figure 4c underscores the key role of the lysine residues in the catalytic mechanism of PFK amyloid fibrils.

To shed further light on the PFK amyloid fibrils' structural features and putative catalytic mechanism, we carried out computational and cryogenic electron microscopy (cryo-EM) analyses (**Figure 5).** Specifically, free molecular dynamics (MD) simulations were performed, illuminating the docking and interactions between PFK and nitrocefin (**Figure 5a**), constituting the initial step of the β-lactam hydrolysis reaction. The calculations utilized as a starting point a naive model of PFK dodecamer, predicted in AlphaFold3[37], with the nitrocefin molecule placed 1.4 nm above the PFK surface. This configuration ensured no biasing of nitrocefin and PFK to a specific initial structure, allowing the system to better scan bound nitrocefin conformations.

The representative conformation in **Figure 5a**, calculated through 1.5 μs in aggregate simulations, reveals a bound conformation of nitrocefin, stabilized by hydrogen bonds between lysine sidechains displayed on the PFK fibrils' surface and carbonyl units in nitrocefin. Notably, the snapshot structure in Figure 5a indicates that nitrocefin complexation occurs via hydrogen bonds between the sidechains of Lys-10 and Lys-12 and nitrocefin carbonyls. It should be noted that the MD simulations yielded bound nitrocefin conformations in which other lysine residues in the PFK sequence partook in hydrogen bond formation. Indeed, the bar diagram in **Figure 5b** depicts the relative probabilities of hydrogen bond formation between nitrocefin and primary amines of the lysine residues, as predicted by the MD simulation analysis. Figure 5b points to preferred binding of nitrocefin to the lysine residues that are close to the C-terminus, presumably due to affinity of nitrocefin to the positively charged terminus. Indeed, electrostatic interactions play an important role in the formation of biological complexes in which Brownian motion limits the rate of encounters between the assembly constituents (nitrocefin and PFK fibrils' surface in this system)[38,39,40]

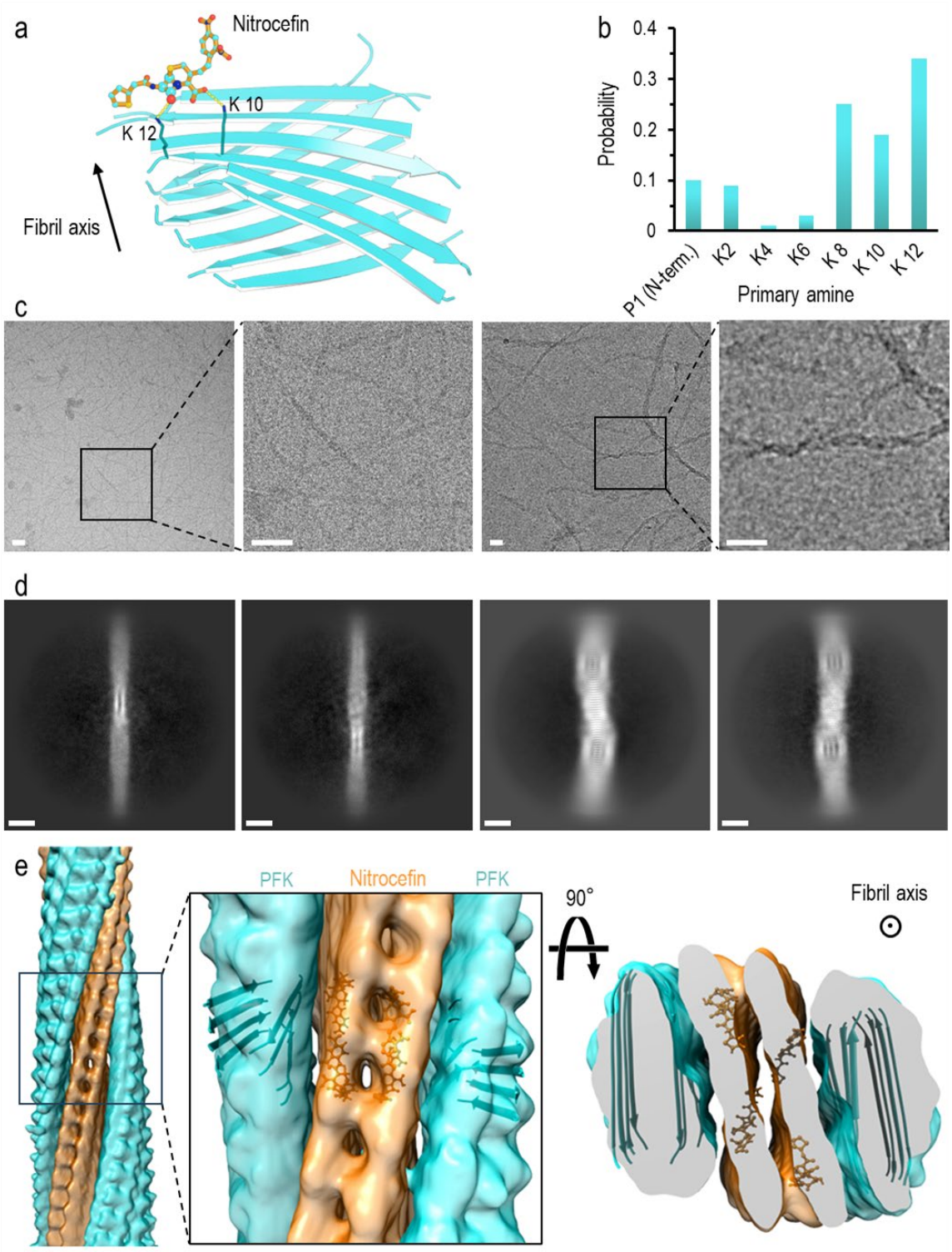

Figure 5. Structural analysis of the PFK fibril / nitrocefin assembly. a. MD-based snapshot of nitrocefin docking on the surface of a PFK fibril, showing hydrogen bonds between nitrocefin and Lys-10 and Lys-12 displayed on the β-sheets. **b.** Relative probabilities of lysine binding to

nitrocefin, extracted from the MD simulations. **c.** Cryo-EM micrographs of PFK fibrils (formed in 0.2 M KCl solution) without nitrocefin (**left)** and following incubation with nitrocefin (0.7 mM; **right)**. Scale bars correspond to 20 nm. **d.** Representative 2D class averages of PFK amyloid fibrils without (two **left** images) and after incubation with nitrocefin (**right** images). Scale bars correspond to 5 nm. **e.** 3D cryo-EM map of PFK fibrils incubated with nitrocefin. Zoomed-in are side (center) and radial (right) views of manually fitted MD-based model to the 3D cryo-EM map. Images were made with UCSF-chimera[41] and PyMol. For more orientations see Figure S8. The 3D map is based on 507,432 analyzed particles.

Cryo-EM analysis furnishes remarkable structural information on the PFK/nitrocefin complexation, complementing the MD simulations, and further illuminating the allosteric catalytic mechanism. The raw micrographs in **Figure 5c** reveal a significant difference between the morphologies of the PFK fibrils with and without nitrocefin. Specifically, the bare PFK amyloid fibrils (without added nitrocefin) form thin single fibers (Figure 5c, left), while thicker, intertwined fiber assemblies can be discerned following incubation with nitrocefin (Figure 5c, right). Representative 2D class averages in **Figure 5d** further highlight the nitrocefin-mediated morphological transformation of the PFK amyloid fibrils. Specifically, while the as-assembled, bare PFK amyloid fibrils feature the parallel β-sheet fiber organization (Figure 5d, two left images)[21], the nitrocefin-incubated sample yielded striated structures comprising coiled double fibril structure exhibiting a 4.9 Å pitch (Figure 5d, right images).

3D helical reconstruction in **Figure 5e**, consisting of 507,432 analyzed particles, yields a unique two coiled fibril morphology, with a twist of -7.35º and a rise of ~12 Å, linked together by the embedded nitrocefin molecules. The map resolution achieved (~5 Å, Figure S9) does not allow for unambiguous side-chain assignment, presumably due to fiber flexibility and hence inherent

heterogeneity between boxed particles. The 90^0-shifted cross section in Figure 5e highlights the double cross-β structures, capable of binding and burying more than one nitrocefin molecule. At this orientation, each fibrillar-component anchors one nitrocefin molecule, and in total two molecules per unit cell, in which the C-termini lysines (K10-K12) are near the embedded nitrocefin substrate. The helically reconstructed structure in Figure 5e is consistent with the MD-derived structure (i.e., Figure 5a), in which the positively charged lysine residues face the polar and negatively charged nitrocefin moieties, consequently generating a pronounced hydrophobic surface stabilizing the double layered PFK fibril/nitrocefin assembly.

We explored practical applications of PFK amyloid-mediated β-lactam hydrolysis, specifically as a vehicle for antibiotic removal in water **(Figure 6).** In the experiments, we coupled PFK fibrils to commercially available silica beads in a column-filter setup and evaluated the degradation capabilities for water containing dissolved β-lactam antibiotics**. Figure 6a** illustrates the experimental scheme. To conjugate the PFK amyloid fibrils with the silica beads, we functionalized PFK with levodopa (L-DOPA) via binding to the amine sidechain of Lys-12 (the peptide is denoted PFK_{DOPA}). The catechol ligand of L-DOPA can be anchored onto the silica beads' surface through bidentate coordinative bonds[42,43]**.** Importantly, bare PFK_{DOPA} fibrils (not coupled to silica beads) readily formed fibrils which also catalyzed β-lactam hydrolysis (Figure S10). The representative scanning electron microscopy (SEM) image of the PFK_{DOPA}/bead in Figure 6a, inset, confirms that bound PFK_{DOPA} fibrils are abundantly displayed on the silica bead surface. The adsorption curve in **Figure 6b,** calculated through the measurement of the UV-vis absorbance of PFK_{DOPA} in the supernatant, further shows the effective attachment of PFK_{DOPA} fibrils, with saturation of the beads' surface occurring at peptide concentrations higher than 3 mM.

Brunauer-Emmett-Teller (BET) analysis indicates a significant increase in the surface area of the PFK_{DOPA}-coated beads, compared to the bare counterparts (Figure S11).

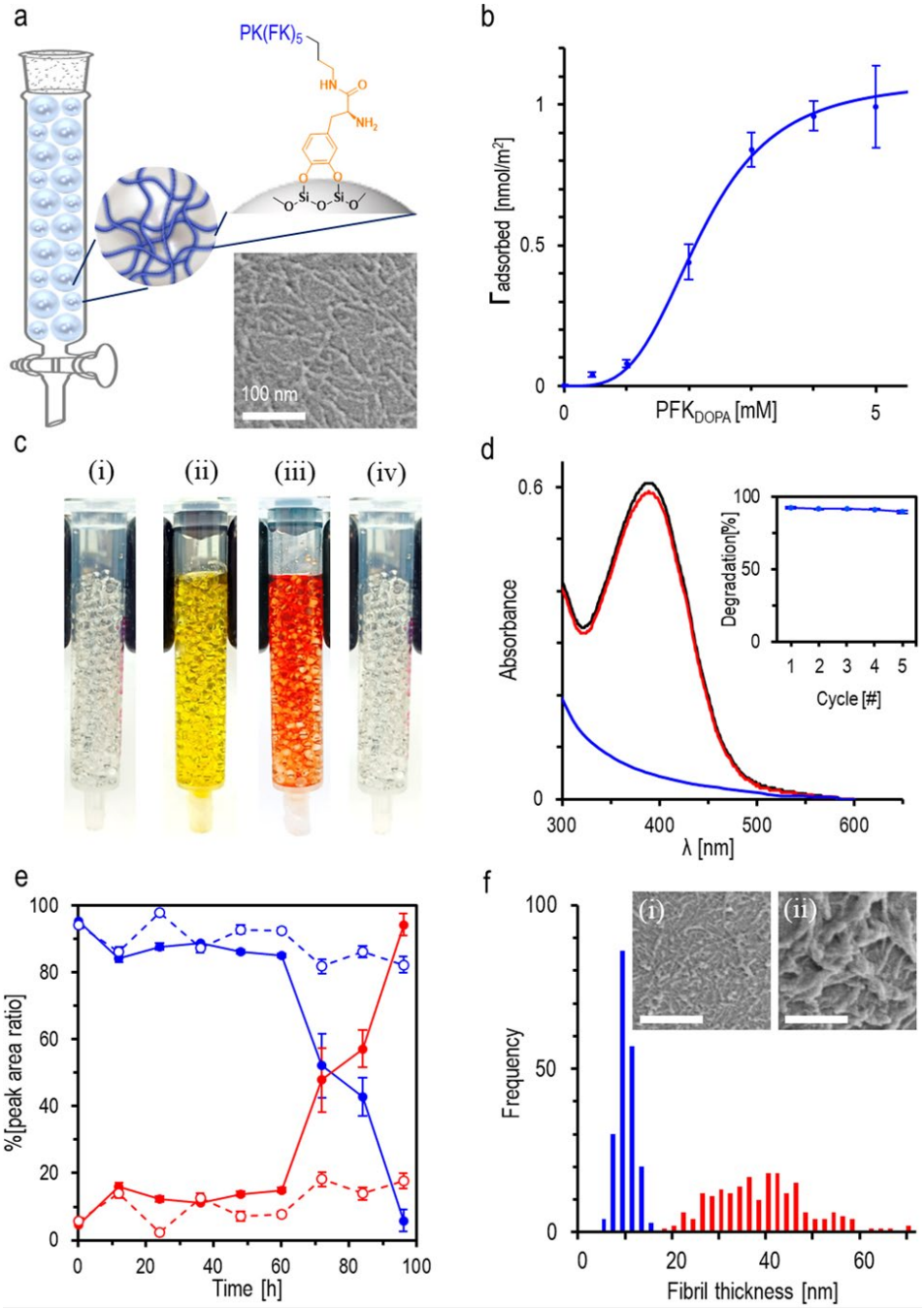

Figure 6. PFK_{DOPA}-silica bead constructs employed for hydrolysis and removal of water-soluble β-lactam antibiotics. a. Illustration of a water filtration column containing PFK_{DOPA} grafter silica beads. PFK_{DOPA}. PFK_{DOPA} anchors onto the silica bead surface via the side chain of

Lys-12. The SEM image depicts abundant PFK_{DOPA} fibrils attached to the bead's surface. **b.** Adsorption isotherm of PFK_{DOPA} fibrils on 10 µm silica particles (50µg/mL particles), determined through the UV-vis absorbance of PFK_{DOPA} in the supernatant, and fitted to the Hill equation using nonlinear regression. **c.** Photographs showing hydrolysis of nitrocefin using the PFK_{DOPA}-bead column filter. i. A glass column filled with PFK_{DOPA}-silica bead (2 mm bead diameter, coated with 3 mM PFK_{DOPA}). ii. The column immediately after addition of nitrocefin solution (200 µM nitrocefin in deionized water). iii. The column after six-hour incubation, indicating pronounced hydrolysis of the nitrocefin. iv. Photograph taken following five cycles of nitrocefin addition and washing with deionized water. **d.** UV-vis absorbance spectra of the eluent - fresh nitrocefin (200 µM) prior to injection into the PFK_{DOPA}-silica bead column (black spectrum), the eluate collected from the column (blue spectrum), and nitrocefin solution eluate after passing through a column of silica beads not coated with PFK_{DOPA} fibrils (red spectrum). The inset shows the percentage of nitrocefin degradation following several cycles of nitrocefin addition. **e.** Hydrolysis of penicillin using the PFK_{DOPA}-silica bead column setup. Relative penicillin concentrations in the eluate were determined by LC-MS (the LC-MS chromatograms are presented in Figure S4). Solid blue curves correspond to non-hydrolyzed penicillin, red curves hydrolyzed penicillin. Broken lines represent control samples using bare silica beads uncoated with PFK_{DOPA}. Each datapoint represents an average of three independent measurements and is presented as the average ± SD, n=3. **f.** SEM images of PFK_{DOPA}-silica bead prior to nitrocefin addition (i), and after five cycles of nitrocefin incubation (ii). Scale bars correspond to 200 nm. Diagram showing fibril width distribution before (blue) and after (red) ten nitrocefin incubation. Fibril width distribution was carried out using ImageJ image analysis software, examining 200 fibrils.

Figure 6c presents a photograph of a 1 cm diameter plastic column containing PFK_{DOPA}-grafted silica beads (2 mm diameter) utilized for hydrolysis of water-soluble nitrocefin. In the experiment, aqueous nitrocefin solution (200 µM) was injected into the filtration column (Figure 6c,ii). Notably, within six hours incubation, the PFK_{DOPA}-grafted silica beads / nitrocefin mixture changed color from yellow to red (Figure 6c,iii), indicating pronounced nitrocefin hydrolysis.

Following flushing the column with distilled water, most of the embedded nitrocefin was removed (the residual reddish appearance in Figure 6c,iv indicates bound hydrolyzed nitrocefin).

The UV-vis absorbance spectra in **Figure 6d** (recorded in samples of 10 μm diameter silica beads) confirm effective nitrocefin hydrolysis following incubation with the PFK_{DOPA}-grafted beads. Specifically, the eluate collected from a PFK_{DOPA}-coated beads column yielded negligible absorbance at 380 nm (Figure 6d, blue), indicating complete hydrolysis. In contrast, both nitrocefin eluent (prior the insertion into the column), and the eluate collected after passage of nitrocefin in a column containing bare silica beads (not displaying PFK_{DOPA}), produced spectra showing the significant nitrocefin signals at 380 nm, indicating no hydrolysis. Figure 6d, inset, demonstrates the recyclability of the coated beads; essentially, ~90% degradation was achieved even after five consecutive cycles, indicating that the PFK_{DOPA} amyloid fibrils attached to the beads remained catalytically active through multiple β-lactam hydrolysis cycles.

We additionally examined whether the PFK_{DOPA}-silica beads catalyze hydrolysis of other β-lactam substrates. **Figure 6e** presents the relative concentration percentage of penicillin and its hydrolysis product, determined via LC-MS, following placing in a column containing PFK_{DOPA}-coated silica beads (10 μm diameter). Indeed, the graphs in Figure 6e demonstrate that incubation of penicillin with the PFK_{DOPA}-coated beads gave rise to significant hydrolysis (almost 95% of the penicillin placed in the column was degraded within 96 hours), while incubation with bare silica beads (not coupled with the PFK_{DOPA} fibrils) did not exhibit hydrolysis. This outcome echoes the result recorded in the case PFK amyloid fibrils alone (e.g., Figure 1d), confirming that the FK_{DOPA}-coated bead constructs can be successfully employed as a vehicle for catalytic β-lactam degradation.

Figure 6f presents SEM analysis of the PFK_{DOPA}-coated silica beads, prior to and after nitrocefin incubation. Specifically, before the introduction of the nitrocefin solution, the PFK_{DOPA} fibrils on the beads' surface were relatively homogeneous, with average diameters of 8 ± 2 nm. However, following 10 nitrocefin incubation cycles, the fibrils' thickness significantly increased, giving rise to 40 ± 10 nm diameters. Indeed, the thick fibrillar species apparent following incubation of the PFK_{DOPA}-coated silica beads with nitrocefin, apparent both in the SEM image and fibril thickness bar diagram in Figure 6f, echo the coiled fibril morphologies recorded by cryo-EM (i.e., Figure 5).

Discussion

Removal of antibiotic substances seeping into wastewater and groundwater is a major public health and environmental challenge. This study depicts an innovative water purification strategy, employing peptide amyloid fibrils as vehicles for catalyzing hydrolysis of β-lactam antibiotics in water. The experiments demonstrate that PFK, an amyloid-forming short peptide comprising alternating lysine/phenylalanine residues and proline termini, displayed efficient hydrolysis of β-lactam substrates, both in its suspended (standalone) fibrillar form, and as fibrils attached to silica beads. Importantly, PFK fibrils catalyzed hydrolysis of different β-lactam substrates: nitrocefin, a β-lactam surrogate, amoxicillin and penicillin which are among the most widely used antibiotic compounds.

The observation that PFK amyloids catalyze β-lactam degradation echoes our recent discovery that PSMα3 amyloid fibrils, biofilm-associated cross-α amyloids secreted by *Staphylococcus aureus*, catalyze β-lactam hydrolysis[16]. Similar to PSMα3, PFK displays nucleophilic lysine arrays at the fibrils' surface[16]. Different than cross-β PFK fibrils, however, PSMα3 adopts a cross-α structure[44] and contains a smaller percentage of lysine residues (four lysine within the 22-residue

sequence), which may account for the significant difference in the catalytic mechanisms between the two systems – allosteric mechanism in the case of PFK vs Michaelis-Menten for PSMα3.

Structural and functional (catalytic) analyses of several modified PFK sequences shed light on the structural determinants and distinct residues contributing to PFK amyloid catalytic activities (Figure 4). The PFK-derived variant analysis confirms that fibril formation is critical for the catalytic activity of PFK. Indeed, the alternating hydrophobic-hydrophilic pattern of PFK has key functional roles: the amphiphilic pattern induces cross-strand fibril architecture, burying the hydrophobic residues while exposing the cationic sidechains. The fibrillar organization further docking of the β–lactam substrates through electrostatic affinity to the lysine sidechains. Indeed, PFK itself was not catalytic in conditions that were not conducive to fibril formation - either low peptide concentrations, or decreased ionic strength (Figure 1); both scenarios promote soluble polyproline type-II structure rather than fibril formation[28,45].

While the peptide variant analysis in Figure 4 attests to the significance of positive fibrils surface charge, the less pronounced catalytic activity of PFR fibrils in comparison with PFK point to the key roles of the lysine sidechains in inducing catalysis. This observation is supported by the MD simulations highlighting the significance of K8, K10, and K12 in anchoring the β-lactam substrate on the PFK amyloid fibril surface. The lysine arrays likely create high local cationic charge on the fibril surface, enhancing immobilization of the anionic β-lactam molecules on the fibril surface. In parallel, the ubiquitous lysine sidechains partake in nucleophilic attacks on the β-lactam rings, resulting in their destabilization and subsequent hydrolysis. The decreased pKa value of the primary amine side chains of the PFK fibrils rather than the peptide monomers (Figure S12) further attests to the enhanced reactivity of the amines on the fibril surface. This model echoes reported

activities of serine nucleophiles in β-lactamases, in which deprotonated serine residues at the active sites act as nucleophiles, forming covalent acyl-enzyme intermediates via the carbonyl units in the β-lactam ring[46]. Other studies reported that metal ions in metal-β-lactamases activate water molecules, which similarly attack the carbonyl residues in the β-lactam ring[47]. In both enzyme systems, a water molecule hydrolyzes the acyl-enzyme intermediates, consequently releasing the inactivated β-lactam substrate. The presumed similarity between the catalytic properties of PFK amyloid fibrils and β-lactamase enzymes is supported by the observation that an anti-β-lactamase polyclonal antibody successfully inhibited PFK amyloid fibril-induced β-lactam hydrolysis (Figure 3).

Further structural insight is furnished through application of cryo-EM, revealing a remarkable β-lactam-induced PFK coiled-fiber organization. This observation underlies the catalytic mechanism, particularly the allosteric behavior. Specifically, the negatively charged nitrocefin substrate initially binds to the PFK fibrils through electrostatic interactions with the lysine sidechains. In higher nitrocefin concentrations, the abundance of negative charge gives rise to inversion of the fibrils' surface potential (apparent in the nitrocefin-dependent ζ-potential analysis, Figure S13) giving rise to complexation of two adjoining PFK amyloid fibrils through the central interweaved nitrocefin array, forming the coiled fibril organization. Importantly, the coiled fibril assembly likely enhances the catalytic activity via nucleophilic attacks of the abundant lysine sidechains on the β-lactam four-member rings of the embedded substrate molecules. Furthermore, the coiled fibrils may accelerate the catalytic activity by creating physical barrier for substrate diffusion, thereby increasing the probability of the substrate to engage with the nucleophilic residues on the PFK fibrils' surface. Notably, recent studies have emphasized the significance of allosteric mechanisms in catalysis induced by short peptide assemblies[48].

Amyloid fibril-catalyzed β-lactam hydrolysis furnishes a useful platform for degradation of antibiotic substances in water (Figure 6). Notably, we demonstrated that the catalytic properties were retained even upon binding and display of the PFK fibrils upon silica beads. As such, the PFK fibril-bead constructs can be readily employed in conventional column filtering apparatuses, allowing both degradation and removal of varied water-soluble β-lactam antibiotics, and recycling of the PFK-bead system for repeated applications. Overall, the use of synthetic, easy to prepare, and environmentally benign catalytic amyloids for eliminating water-soluble β-lactam antibiotics is a promising technology addressing the major environmental and health challenge of antibiotic water contamination.

Conclusions

This study demonstrates that amyloid fibrils of a *de-novo* designed peptide, PFK, serve as effective catalysts for the hydrolysis of β-lactam antibiotics. The catalytic activity of PFK amyloid fibrils occurs via a unique allosteric mechanism, mediated through formation of a coiled double fiber organization embedding the β-lactam substrate molecules and facilitating nucleophilic attacks by the sidechains of the lysine residues. PFK amyloid fibrils successfully catalyzed hydrolysis of varied β-lactams, including nitrocefin, amoxicillin, and penicillin, underscoring the generic nature of the catalytic platform. Practical utilization of the catalytic amyloids was further manifested through the display of the PFK fibrils on silica beads and usage of the amyloid fibril/bead constructs for water decontamination in a conventional filtration column. In conclusion, PFK catalytic amyloids furnish an innovative strategy for degradation of antibiotics in water, offering means for addressing this major environmental and health hazard.

Experimental Section

Materials

Hepes (4-(2-hydroxyethyl)-1-piperazineethanesulfonic acid, >99% purity) and Nitrocefin (3-(2,4-Dinitrostyryl)-(6R,7R)-7-(2-thienylacetamido)-ceph-3-em-4-carboxylic Acid, M.W of 516.50) were purchased from Holland-Moran (Yehud, Israel). Ammonium acetate (99% purity) Potassium chloride (99% purity) and 1,1,1,3,3,3-Hexafluoro-2-propanol (HFIP, 99% purity), amoxicillin (95% purity) and Penicillin G sodium salt (96% purity) were purchased from Sigma-Aldrich (Rehovot, Israel). Acetonitrile (LC-MS grade, 99.9% purity) was obtained from Beith Dekel (Raanana, Israel, Manufactured by JTBaker). The fluorescent dye Amytracker-680 was supplied by Ebba biotech (Stockholm, Sweden). Glass beads of 2 mm dimeter were purchased from Mercury (Darmstadt, Germany),and silica microparticles in diameter of 10 μm were purchased from microparticles GmbH (Volmerstraße, Berlin). Anti-β-lactamase (polyclonal anti-β-lactamase, with affinity to β-lactamase of E.Coli, LOT AB3738-I, UniProt P62593) was purchased from Mercury (Darmstadt, Germany).

Peptide preparation

The peptide Pro-Lys-(Phe-Lys)$_5$-Pro (Mw of 1717.14; **PFK**), Pro-Arg-(Phe-Arg)$_5$-Pro (Mw of 1885.25; **PFR**), Pro-Ser-(Phe-Ser)$_5$-Pro (Mw of 1470.60; **PFS**), Pro-Asp-(Phe-Asp)$_5$-Pro (Mw of 1638.65; **PFD**), Pro-Asp-(Phe-Lys-Phe-Asp)$_2$-Phe-Lys-Pro (Mw of 1677.90; **PFDK)**, Lys-Phe-Phe-Pro-Lys-Lys-Pro-Phe-Lys-Phe-Phe-Lys-Lys, (Mw of 1877.33; **ScFK**), DOPA-Lys-(Phe-Lys)$_5$-Pro (Mw of 1799.22; **PFK$_{DOPA}$**) were custom-synthesized and purified to 95% by HPLC and supplied as lyophilized powder. PFK and PFK$_{DOPA}$ were synthesized and supplied by GL Biochem (Shanghai, Chaina). PFD was supplied by American Peptides (Sunnyvale, CA, USA).

PFR, PFS, PFDK, and ScFK and were supplied by GenScript (Piscataway, NJ, USA). The accurate peptide content was analyzed by the suppliers and the actual amounts and concentration in the experiments were calculated accordingly.

The lyophilized peptides were dissolved at 0.2 mM concentration in Hepes buffer (50 mM) and pH 7.4. The buffered peptide solutions were vortexed until transparent clear solutions were obtained. The solutions were supplemented with concentrated KCl aqueous solution (0.6 M) to final peptide concentrations of 0.2 mM and KCl concentration of 0.3 M. The peptide samples were let to equilibrate at room temperature for two hours and the solutions diluted to the desired concentrations using the same buffer. All peptide solutions and buffers were prepared using deionized water (DIW, 18.2 MΩcm, Barnstead Smart2Pure, Thermo Scientific, MA, USA).

Amytracker-680 fluorescence

Peptide samples (PFK and variants) were prepared as described above and diluted to a final concentration of 0.2 mM using Hepes buffer at a concentration of 50 mM, pH 7.4. A solution of Amytracker-680 fluorescent dye was prepared by diluting the dye by 50 folds in DIW. 45 µL of each peptide sample were placed in a 384-well black plate and supplemented with 5 µL of Amytracker-680 solution (total dilution of Amytracker-680 in the sample upon mixing, x500 times, 0.002 mg/mL). The samples within the plate were incubated for 10 more minutes before fluorescence measurements. The samples' fluorescence was measured using a Biotek Synergy H1 plate reader (Biotek, Winooski, VT, USA) using 550 nm excitation and 650 nm emission.

Cryogenic transmission electron microscopy (cryo-TEM)

5µL droplets of each peptide solution (0.2 mM), prepared as described above, were deposited onto a glow-discharged TEM grid (300 mesh Cu Lacey substrate grid; Ted Pella). Excess liquid was

removed by automatic blotting with filter paper, and the samples were plunged into liquid ethane precooled with liquid nitrogen in a controlled environment using a Leica EM GP apparatus. Vitrified samples were then transferred to a cryo-specimen holder and examined at −181 °C using a FEI Talos S200C microscope operating at 200 kV in low-dose mode. Images were captured using a Ceta camera (4k × 4k) and analyzed using Digital Micrograph software by Gatan Inc.

Nitrocefin hydrolysis kinetics

Nitrocefin stock solution (20 mM) was prepared in acetonitrile and then diluted with Hepes buffer (50 mM, pH 7.4) to a concentration of 2 mM (further dilutions were made from this stock). All nitrocefin samples were kept on ice, and subsequent dilutions or mixing were performed under cold conditions to prevent background self-hydrolysis. Pre-cooled nitrocefin solutions (50 µL) were mixed with pre-incubated PFK solutions (200 µM PFK, incubated in Hepes 50 mM, KCl 0.2 M, pH 7.4) in pre-cooled clear 96-well plates (Greiner flat-bottom; 360 µL). The plate was then transferred to a pre-cooled plate reader (Multiskan GO, Thermo Scientific, Waltham, MA) at 18°C and shaken slowly for 5 seconds. The absorbance of degraded nitrocefin was measured every 1 minute at λ=480 nm for two hours. Initial rates (V_0) were calculated based on the slope of the initial linear range of degraded nitrocefin production within the first 15 minutes. Reported results represent the average of at least five separate measurements (N, the exact number of repeats, is provided). Each experiment included blank samples of nitrocefin substrate diluted with buffer instead of PFK. All presented results were adjusted for buffer control subtraction. Initial rate calculations also accounted for substrate self-degradation, ensuring that product absorbance resulted from the presence of PFK.

Kinetic data analysis

The initial rates of degraded nitrocefin generation, derived from the slopes within the first 15 minutes as described earlier, were subjected to non-linear regression analysis using the solver function in Excel. This analysis involved fitting the initial rates (V_0) to the Hill equation:

$$V = \frac{V_{max}[s]^h}{(K_h^h + [s]^h)}$$

V_{max} represents the maximum reaction rate, K_h represents the weighted affinity in the Hill equation, [S] signifies the substrate initial molar concentration, and h is the Hill coefficient. Each initial rate value was expressed as an average ± SEM. The kinetic parameters were determined by fitting the data to the Hill model using non-linear regression, with confidence intervals computed for each parameter accordingly using excel (Microsoft office 365 ProPlus).

Liquid chromatography - mass spectrometry (LC-MS)

Antibiotic solutions were dissolved in LC-MS grade water at a concentration of 60 µM. 100 µL of the antibiotic solution was added to the fibrils/fibrils'-coated beads, and 5 µL of the solution were collected in time intervals of 0, 12, 24, 36, 48, 60, 72, 84 and 96 hours. The collected samples were immediately mixed with 95 µL of organic solvent to quench the catalytic reaction (acetonitrile for amoxicillin, methanol for penicillin). The samples were centrifuges, transferred to the LC-vials, and injected sequentially for the LC-MS analysis. The analysis was performed on Waters ACQUITY UPLC I-Class PLUS System equipped with Acquity UPLC BEH C18 column (1.7µm, 2.1 x 50mm) coupled with high-resolution Orbitrap Exploris 240 mass-spectrometer (Thermo scientific, MA, USA) equipped with electro-spray ionization source. The chromatography separation was achieved by gradient of the mobile phase A (0.1% formic acid) and mobile phase B (acetonitrile) in the following 0-5 min 90% of A, 5-7.5 min 40% of A, 7.5-10 min 10% of A,

10-12 min 10% of A, 12-13 min 90% of A, 13-15 min 90% of A. The flow rate was 0.4 mL/min, and the column temperature was 40°C. The parameters of the MS were set according to the manufacture recommendations. The samples were analyzed in a full-scan mode (70-1000 m/z) with 140,000 FWHM resolution. Relative abundance of the intact/degraded compounds was calculated by the peak area of the extracted ion chromatogram: for amoxicillin 366.1-366.12 m/z, for degraded-amoxicillin 384.1-384.13 m/z, for penicillin 335.1-335.12 m/z, and for degraded-penicillin 353.1-353.12 m/z. The data was analyzed using Xcalibur software, v4.2 (Thermo Fisher Scientific, California, USA).

Inhibition of PFK-fibrils catalytic activity with anti-β-lactamase polyclonal antibodies

PFK fibrils were prepared as described above at a concentration of 5 mM (above the critical assembly concentration, CAC) by dissolving the peptide in a Hepes buffer (50 mM Hepes, pH 7.4) and incubating for 2h at room temperature. The peptide solution was prepared without salt co-addition to avoid high salinity that might affect the antibody functionalities. In the experiment, we co-incubated PFK fibrils, nitrocefin, and an anti-β-lactamase rabbit polyclonal antibody (*E.coli* anti-β-lactamase rabbit polyclonal antibodies, UniProt number MM_NF-AB3738-I) at a concentration ratio of 2000/333/4.6 for PFK/nitrocefin/anti-β-lactamase. Anti-β-lactamase antibodies at a 360 μg/mL concentration were mixed with the PFK solution obtaining a final antibody concentration of 4.6 μM (144 μg/mL) and 2 mM PFK concentration. Fresh nitrocefin at a concentration of 333 μM was co-added with the PFK fibrils, either and or without anti-β-lactamase antibodies using 10 μL of antibody solution (144 μg/mL) were mixed with 10 μL of PFK fibril solution. The samples were placed in clear 384-well plate and the absorbance of the degraded nitrocefin was recorded every minute using plate reader (Biotek, Waltham, MA, USA) at a wavelength of λ=480 nm over two hours. The reported findings reflect the average of no less

than three independent experiments. All results presented have been adjusted to account for buffer control subtraction.

For kinetic analysis of antibody effect, 10 µL solutions of preincubated PFK fibrils (3 mM) were placed in a clear 384-well plate-reader (Greiner flat-bottom), and 15 µL anti-β-lactamase (stock solution concentration of 500 µg/mL) was added and serially diluted by 2/3. Prior to the measurement, the plates were cooled and kept on ice. Nitrocefin solutions in concentration of 1 mM and volume of 5 µL were then added into each well and the plate was transferred to a pre-cooled plate reader (T=18ºC, Multiskan GO, Thermo Scientific, Waltham, MA) and the plate was shaken for 5 seconds. The absorbance of degraded nitrocefin was measured every 1 minute at λ=480 nm for two hours. Reported results represent the average of at least three separate measurements (the exact number of repeats is provided). Each experiment included negative-control of nitrocefin substrate diluted with buffer without PFK, and positive control of PFK lacking anti-β-lactamase. All presented results were adjusted for buffer control subtraction.

ζ-potential measurements

ζ-potential of the peptide variant assemblies was measured using a Zetasizer (Zetasizer Nano ZS, Malvern, Worcestershire, UK) using Malvern DTS 1070 disposable U-shape capillary cuvettes. 1 mL of PFK variants sample, containing preformed fibrils in concentration of 0.2 mM were prepared as described above (Hepes 50 mM pH 7.4, KCl 0.2 M) The values are presented as an average±SEM, n=5.

Molecular dynamics (MD) simulations of nitrocefin binding to modelled PFK-fibrils

Systems building and simulation steps

Initial 3D model of PFK was built using AlphFold3 server[50]. The 3D model was used to build 6 naïve systems, composed of PFK and nitrocefin. For each system, PFK model composed of 12 repetitions of the peptide was placed in simulation box with the size of 5.2 nm × 4 nm × 10 nm. In each system, a nitrocefin molecule was randomly placed at least 1nm from the peptide. Each system was then solved using water and was charge-neutralized using Cl- ions. To mimic the experimental conditions, 0.35 M of NaCl was added before subjecting the system to energy minimization using the steepest descent method. The energy-minimized systems were then subjected to temperature equilibration for 200 ps at 300K (NVT). Following temperature equilibrium, all systems were equilibrated for 1 bar pressure for 200 ps (NPT). Finally, all systems were subjected to a production run for a period of 300 ns without any restraints. Analysis of the MD run was performed using the in-built tools of GROMACS, and figures were plotted using PyMOL Molecular Graphics System, Version 3.0 Schrödinger, LLC.

Molecular dynamics simulation settings

The Amber14SB_OL15 force field was used to described peptides[51] and the TIP3P model[52] was used for the water. The topology and parameters of nitrocefin were generated using the ACPYPE web server[53] with GAFF atom types. Water All simulations were run using the GROMACS 2023.4 software[54]. The PME method was used for calculating long-range electrostatic interactions[55], with a cut-off distance of 1.2 nm, was used for short-range repulsive and attractive interactions. All bonds involving hydrogen atoms were constrained with the LINCS algorithm[56]. Temperature was kept constant - at 300K – using the velocity rescale scheme[57] coupling parameters of 1.0 ps^{-1}. The Parrinello-Rahman[58] 0.2 algorithm was used to maintain the pressure of the system at 1 bar with a coupling constant of τ = 5.0 ps.

Cryo-electron microscopy (cryo-EM)

Cryo-EM was carried out on samples prepared by depositing 3 μL solution of PFK assemblies (0.2 mM peptide concentration) on glow-discharged Quantifoil R 1.2/1.3 holey carbon grids (Quantifoil Micro Tools GmbH, Germany). Samples were manually blotted for three seconds at room temperature following vitrification by rapidly plunging into liquid ethane using a home-built plunging apparatus. The frozen samples were stored in liquid nitrogen until imaging. For imaging the samples were loaded under cryogenic conditions and imaged in low-dose mode on a Glacios microscope (Thermo-Fisher) operated at 200 kV. Automated data collection was done using EPU (Thermo-Fisher). Movies were collected at a calibrated pixel size of 0.89 Å by a Falcon4i direct electron detector fitted behind a Selectris X energy filter (Thermo-Fisher) set to ±5 eV around zero-loss peak. The detector was operated in a dose fractionated counting mode, at a dose rate of 8 $\bar{e}$/pixel/second, with a total electron dose of 30 $\bar{e}$/Å^2. Data was collected at a defocus range of -0.5 to -1.5 μm. All processing was done using cryoSPARC v4.3.0.[51] Dose-fractionated movie stacks were patch-motion corrected, and their defocus values were estimated. The aligned sum images were used for further processing. Particles were picked using filament tracer followed by extraction of 500 pix long overlapping segments (with a shift of 2 times of the expected axial rise). 2D class averages were manually selected and used for further 3D refinement. All selected classes had clear signatures of the four-layered pattern. Ab-initio reconstruction of three classes was used to prepare an initial map. Helical parameters of -7.35° twist and 12.0 Å rise, calculated using symmetry search, were used to reconstruct the final 3D map.

Adsorption Isotherms of PFK$_{DOPA}$ on silica beads

PFK$_{DOPA}$ adsorption onto the silica beads was analyzed using adsorption isotherms: 10 μm-diameter silica beads ((Volmerstraße, Berlin) were washed extensively with 0.1 M HCl, 0.1 M KOH and followed by three washing cycles with DIW to remove surface-bound groups. The beads

were then co-incubated with preformed PFK_{DOPA} fibrils solutions at various concentrations (0, 0.45 mM, 1 mM, 2 mM, 3 mM, 4 mM, and 5 mM), prepared in Hepes buffer (50 mM, pH 7.4) supplemented with 0.6M KCl. The samples were incubated for 2h at room temperature. 100 µL of the preformed fibrils solutions were co-incubated with 50 µg beads. Following this, 50 µL of the supernatant solution was collected and transferred to clear UV-Star 96-well plates (Greiner flat-bottom), and the absorbance was measured at λ=258 nm using Biotek Synergy H1 plate reader (Biotek, Winooski, VT, USA).

β-lactam hydrolysis using PFK_{DOPA} - grafted beads

A column-filter was prepared using silica beads in diameter of 10 µm, cleaned as described above. 100 µL solution of PFK_{DOPA} fibrils at a concentration of 3 mM, prepared as described above in Hepes buffer (50 mM, pH 7.4, KCl 0.6 M) was co-incubated for 2h with the pre-coated silica beads. The beads were subsequently centrifuged and separated, and washed three times with DIW to remove PFK_{DOPA}/salt leftovers. The coated and washed beads were inserted into a 3 mL plastic-syringe, fitting the volume of the syringe.

Fresh nitrocefin buffered solution at a concentration of 2 mM and volume of 1 mL was injected into the filter column. After 6h, the nitrocefin elution was collected and a sample of 50 µL was placed in clear UV-Star 96-well plates (Greiner flat-bottom). The plate was transformed to Biotek Synergy H1 plate reader (Biotek, Winooski, VT, USA) and the absorbance was recorded at λ= 380 nm, detecting the non-reacted nitrocefin. A similar analysis was performed using penicillin and amoxicillin, dissolved in DIW at a concentration of 60 µM. 100 µL of each antibiotic-solution was added to the column and elution solutions were collected in 5 µL drops, in time intervals of 0, 12, 24, 36, 48, 60, 72, 84, 96, 110 and 132 hours. Immediately after the collection of the elution

samples they were mixed with 95 µL organic solvent to quench the spontaneous hydrolysis reactions (acetonitrile for amoxicillin, methanol in the case of penicillin). The samples were injected sequentially into the LC-MS analysis as described above.

Scanning electron microscopy (SEM)

Pre-coated silica beads were prepared as described above, washed with water and cryogenically snap-frozen by dipping in liquid nitrogen and lyophilized at -30˚C to preserve the secondary structure of the fibrils (LABCONCO-Triad, Labotal, Israel). The samples were imaged at an acceleration voltage of 2.00 kV in Gemini 300 field emission scanning electron microscope (ZEISS, Jena, Germany) equipped with the Everhart-Thornley Secondary Electron detector.

Acknowledgements

The measurements of electron microscopy, FTIR and LC-MS were performed at the Ilse Katz Institute (IKI) for Nanoscale Science and Technology Ben-Gurion University of the Negev, Beer Sheva, Israel. The authors are thankful to Dr. Einat Nativ-Roth for helping with the cryogenic TEM experiments and SEM experiments, Dr. Alexander Upcher for assistance with the microscopy measurements and Dr. Sofiya Kolusheva for her helpful discussions and critical thoughts. The authors are grateful for the generous support from the Guzik Foundation to BGU's Cryo-electron microscopy unit. S.M.K is grateful for the support and funding of IKI. E.A. is thankful to the European Molecular Biology Organization (EMBO) and Yad Hanadiv foundation (the Rothschild foundation).

ASSOCIATED CONTENT

Supporting Information:

The following files are available free of charge.

Figure S1. Effect of salt concentration on PFK-Amytracker fluorescence

Figure S2. Circular dichroism (CD) spectroscopy of PFK

Figure S3. Fourier transform infrared spectroscopy (FTIR) of PFK

Figure S4. LC Gradient program, LC-MS chromatogram and mass spectra of Penicillin degradation reaction.

Figure S5. LC Gradient program, LC-MS chromatogram and mass spectra of amoxicillin degradation reaction

Figure S6. Circular Dichroism (CD) spectroscopy of PFK-homologous and Fourier transform infrared spectroscopy (FTIR) of PFK-homologous.

Figure S7. Nitrocefin degradation by PFK homologous.

Figure S8. Single particle analysis of cryo-EM images: Filament sample processing.

Figure S9. Cryo-EM filament analysis.

Figure S10. Nitrocefin degradation by PFK_{DOPA}

Figure S11. B.E.T of coated and uncoated beads

Figure S12. pH titration of PFK

Figure S13. Inversion of surface potential of PFK with nitrocefin.

AUTHOR INFORMATION

Corresponding Author

Raz Jelinek, E-mail: Razj@bgu.ac.il

Author Contributions

E.A, S.M.K and R.J designed the research; S.M.K performed the experiments involving the synthetic peptides and derivatives (β-lactam degradation kinetics, LC-MS, CD spectroscopy, FTIR spectroscopy, Cryo-TEM sample preparation, SEM sample preparations, ζ-potential

measurements, Fluorescent labelling, Anti-β-lactamase reactions, filtration experiments and others). E.A. performed the preliminary experiments, designed and initiated the project, and contributed to cryo-TEM sample preparation; A.B developed the LC-MS methodology; I.K. performed the MD simulations, R.Z. performed the structural analysis of the peptides using cryo-TEM through single particle analysis. H.R, and R.J supervised the research. S.M.K, E.A, I.K, R.Z. and R.J wrote the manuscript. All authors have commented and given approval to the final version of the manuscript.

Competing interests

The authors declare no competing interests.

REFERENCES

1. Hernando-Amado, S., Coque, T. M., Baquero, F. & Martínez, J. L. Defining and combating antibiotic resistance from One Health and Global Health perspectives. *Nat. Microbiol.* **4**, 1432–1442 (2019).
2. Liu, C., Tan, L., Zhang, L., Tian, W. & Ma, L. A Review of the Distribution of Antibiotics in Water in Different Regions of China and Current Antibiotic Degradation Pathways. *Front. Environ. Sci.* **9**, 1–24 (2021).
3. de Ilurdoz, M. S., Sadhwani, J. J. & Reboso, J. V. Antibiotic removal processes from water & wastewater for the protection of the aquatic environment - a review. *J. Water Process Eng.* **45**, 102474 (2022).
4. Feng, G., Huang, H. & Chen, Y. Effects of emerging pollutants on the occurrence and transfer of antibiotic resistance genes: A review. *J. Hazard. Mater.* **420**, 126602 (2021).
5. Cars, O. *et al.* Resetting the agenda for antibiotic resistance through a health systems perspective. *Lancet Glob. Heal.* **9**, e1022–e1027 (2021).

6. Maurer-Stroh, S. *et al.* Exploring the sequence determinants of amyloid structure using position-specific scoring matrices. *Nat. Methods* **7**, 237–242 (2010).

7. Zozulia, O., Dolan, M. A. & Korendovych, I. V. Catalytic peptide assemblies. *Chem. Soc. Rev.* **47**, 3621–3639 (2018).

8. Arad, E., Baruch Leshem, A., Rapaport, H. & Jelinek, R. β-Amyloid fibrils catalyze neurotransmitter degradation. *Chem Catal.* **1**, 908–922 (2021).

9. Arad, E., Yosefi, G., Bitton, R., Rapaport, H. & Jelinek, R. *Native glucagon amyloids catalyze key metabolic reactions*. (2022).

10. Horvath, I., Mohamed, K. A., Kumar, R. & Wittung-Stafshede, P. Amyloids of α-Synuclein Promote Chemical Transformations of Neuronal Cell Metabolites. *Int. J. Mol. Sci.* **24**, (2023).

11. Wittung-Stafshede, P. Chemical catalysis by biological amyloids. *Biochem. Soc. Trans.* **0**, 1–8 (2023).

12. Horvath, I. & Wittung-Stafshede, P. Amyloid Fibers of α-Synuclein Catalyze Chemical Reactions. *ACS Chem. Neurosci.* **14**, 603–608 (2023).

13. Arad, E. & Jelinek, R. Catalytic physiological amyloids. in (2024). doi:10.1016/bs.mie.2024.01.014.

14. Arad, E. & Jelinek, R. Catalytic amyloids. *Trends Chem.* (2022) doi:10.1016/j.trechm.2022.07.001.

15. Chatterjee, A., Goswami, S., Kumar, R., Laha, J. & Das, D. Emergence of a short peptide based reductase via activation of the model hydride rich cofactor. *Nat. Commun.* **15**, 4515 (2024).

16. Arad, E. *et al.* Staphylococcus aureus functional amyloids catalyze degradation of β-lactam

antibiotics. *Nat. Commun.* (2023) doi:https://doi.org/10.1038/s41467-023-43624-1.

17. Sawazaki, T., Sasaki, D. & Sohma, Y. Catalysis driven by an amyloid–substrate complex. *Proc. Natl. Acad. Sci.* **121**, (2024).

18. Singh, A., Goswami, S., Singh, P. & Das, D. Exploitation of Catalytic Dyads by Short Peptide-Based Nanotubes for Enantioselective Covalent Catalysis. *Angew. Chemie Int. Ed.* **62**, (2023).

19. Rapaport, H., Kjaer, K., Jensen, T. R., Leiserowitz, L. & Tirrell, D. A. Two-Dimensional Order in β-Sheet Peptide Monolayers. *J. Am. Chem. Soc.* **122**, 12523–12529 (2000).

20. Vinod, T. P. *et al.* Transparent, conductive, and SERSactive Au nanofiber films assembled on an amphiphilic peptide template. *Nanoscale* **5**, 10487 (2013).

21. Cohen-Erez, I. & Rapaport, H. Coassemblies of the Anionic Polypeptide γ-PGA and Cationic β-Sheet Peptides for Drug Delivery to Mitochondria. *Biomacromolecules* **16**, 3827–3835 (2015).

22. Ben Ghedalia-Peled, N., Cohen-Erez, I., Rapaport, H. & Vago, R. Aggressiveness of 4T1 breast cancer cells hampered by Wnt production-2 inhibitor nanoparticles: An in vitro study. *Int. J. Pharm.* **596**, 120208 (2021).

23. Cohen-Erez, I., Harduf, N. & Rapaport, H. Oligonucleotide loaded polypeptide-peptide nanoparticles towards mitochondrial-targeted delivery. *Polym. Adv. Technol.* **30**, 2506–2514 (2019).

24. Charles, C. *et al.* Mitochondrial responses to organelle-specific drug delivering nanoparticles composed of polypeptide and peptide complexes. *Nanomedicine* **15**, 2917–2932 (2020).

25. Yosefi, G., Cohen-Erez, I., Nativ-Roth, E., Rapaport, H. & Bitton, R. Spontaneous

Alignment of Self-Assembled Cationic and Amphiphilic β-Sheet Peptides. *Adv. Mater. Interfaces* **7**, 2000332 (2020).

26. Morten, M. J. *et al.* Quantitative super-resolution imaging of pathological aggregates reveals distinct toxicity profiles in different synucleinopathies. *Proc. Natl. Acad. Sci.* **119**, 1–12 (2022).

27. Arad, E., Malishev, R., Rapaport, H. & Jelinek, R. Membrane Determinants Affect Fibrillation Processes of β-Sheet Charged Peptides. *Biomacromolecules* **19**, 307–314 (2018).

28. Arad, E. *et al. A matter of charge : Electrostatically tuned coassembly of amphiphilic peptides*. https://chemrxiv.org/engage/chemrxiv/article-details/663a5d48418a5379b0aedfae doi:10.26434/chemrxiv-2024-jztjq.

29. Viswanatha, T., Marrone, L., Goodfellow, V. & Dmitrienko, G. I. Assays for B-Lactamase Activity and Inhibition. in *Methods in molecular medicine* vol. 142 239–260 (2008).

30. Lima, L. M., Silva, B. N. M. da, Barbosa, G. & Barreiro, E. J. β-lactam antibiotics: An overview from a medicinal chemistry perspective. *Eur. J. Med. Chem.* **208**, 112829 (2020).

31. Mitchell, S. M., Ullman, J. L., Teel, A. L. & Watts, R. J. pH and temperature effects on the hydrolysis of three β-lactam antibiotics: Ampicillin, cefalotin and cefoxitin. *Sci. Total Environ.* **466**–**467**, 547–555 (2014).

32. Weiss, J. N. The Hill equation revisited: uses and misuses. *FASEB J.* **11**, 835–841 (1997).

33. Herve, G. *Allosteric Enzymes*. *Allosteric Enzymes* (CRC Press, 1989). doi:10.1201/9781003068563.

34. Gohara, D. W. & Di Cera, E. Allostery in trypsin-like proteases suggests new therapeutic strategies. *Trends Biotechnol.* **29**, 577–585 (2011).

35. W. F. DeGrado and J. D. Lear. Peptide Conformation at Apolar/Water Interfaces 1. A study with Model Peptides of Defined Hydrophobic Periodicity. *J. Am. Chem. Soc.* **107**, 7684–7689 (1985).

36. Baruch Leshem, A., Zarzhitsky, S. & Rapaport, H. Functional Peptide Monolayers at Interfaces. *Isr. J. Chem.* **55**, 661–670 (2015).

37. Abramson, J. *et al.* Accurate structure prediction of biomolecular interactions with AlphaFold 3. *Nature* 1–3 (2024).

38. Kiel, C., Serrano, L. & Herrmann, C. A detailed thermodynamic analysis of ras/effector complex interfaces. *J. Mol. Biol.* **340**, 1039–1058 (2004).

39. Kukić, P. & Nielsen, J. E. Electrostatics in proteins and protein–ligand complexes. *Future Med. Chem.* **2**, 647–666 (2010).

40. Fersht, A. *Structure and mechanism in protein science: a guide to enzyme catalysis and protein folding*. (Macmillan, 1999).

41. Pettersen, E. F. *et al.* UCSF Chimera—A visualization system for exploratory research and analysis. *J. Comput. Chem.* **25**, 1605–1612 (2004).

42. Herbert, J. *et al.* Mussel Adhesion: Finding the Tricks Worth Mimicking. *J. Adhes.* **81**, 297–317 (2005).

43. Maier, G. P., Rapp, M. V., Waite, J. H., Israelachvili, J. N. & Butler, A. Adaptive synergy between catechol and lysine promotes wet adhesion by surface salt displacement. *Science (80-.).* **349**, 628–632 (2015).

44. Tayeb-Fligelman, E. *et al.* The cytotoxic Staphylococcus aureus PSMa3 reveals a cross-α amyloid-like fibril. *Science (80-.).* **355**, 831–833 (2017).

45. Arad, E., Malishev, R., Rapaport, H. & Jelinek, R. Membrane Determinants Affect

Fibrillation Processes of β-Sheet Charged Peptides. *Biomacromolecules* **19**, 307–314 (2018).

46. Fröhlich, C. *et al.* Epistasis arises from shifting the rate-limiting step during enzyme evolution of a β-lactamase. *Nat. Catal.* 1–11 (2024).

47. King, D. T., King, A. M., Lal, S. M., Wright, G. D. & Strynadka, N. C. J. Molecular mechanism of avibactam-mediated β-lactamase inhibition. *ACS Infect. Dis.* **1**, 175–184 (2015).

48. Roy, S., Laha, J., Reja, A. & Das, D. Allosteric Control of the Catalytic Properties of Dipeptide-Based Supramolecular Assemblies. *J. Am. Chem. Soc.* (2024) doi:10.1021/jacs.4c06447.

49. Voth, K. *et al.* Structural and functional characterization of Legionella pneumophila effector MavL. *Biomolecules* **11**, 1802 (2021).

50. Abramson, J. *et al.* Accurate structure prediction of biomolecular interactions with AlphaFold 3. *Nature* **630**, 493–500 (2024).

51. Punjani, A., Rubinstein, J. L., Fleet, D. J. & Brubaker, M. A. cryoSPARC: algorithms for rapid unsupervised cryo-EM structure determination. *Nat. Methods* **14**, 290–296 (2017).

52. Jorgensen, W. L., Chandrasekhar, J., Madura, J. D., Impey, R. W. & Klein, M. L. Comparison of simple potential functions for simulating liquid water. *J. Chem. Phys.* **79**, 926–935 (1983).

53. Kagami, L., Wilter, A., Diaz, A. & Vranken, W. The ACPYPE web server for small-molecule MD topology generation. *Bioinformatics* **39**, (2023).

54. Abraham, M. J. *et al.* GROMACS: High performance molecular simulations through multi-level parallelism from laptops to supercomputers. *SoftwareX* **1**–**2**, 19–25 (2015).

55. Darden, T., York, D. & Pedersen, L. Particle mesh Ewald: An N ·log(N) method for Ewald sums in large systems. *J. Chem. Phys.* **98**, 10089–10092 (1993).

56. Hess, B. P-LINCS: A Parallel Linear Constraint Solver for Molecular Simulation. *J. Chem. Theory Comput.* **4**, 116–122 (2008).

57. Bussi, G., Donadio, D. & Parrinello, M. Canonical sampling through velocity rescaling. *J. Chem. Phys.* **126**, (2007).

58. Parrinello, M. & Rahman, A. Polymorphic transitions in single crystals: A new molecular dynamics method. *J. Appl. Phys.* **52**, 7182–7190 (1981).

ToC Graphical Abstract:

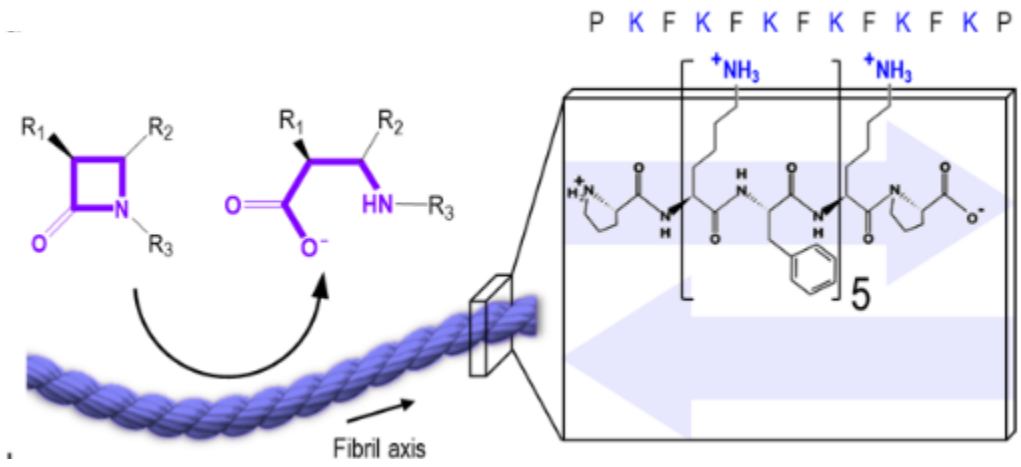

Associated Content:

Coiled double amyloid-like fibrils allosterically catalyze hydrolysis of β-lactam antibiotics

Sisira Mambram Kunnath[1,2#], Elad Arad[1,2,3#], Ran Zalk[1], Itamar Kass[1], Albert Batushansky[1]

*Hanna Rapaport[1,4] and Raz Jelinek[1,2]**

Table of Contents

The following files are available free of charge.

Video:

https://www.dropbox.com/scl/fi/4cqkwouiai48vkcoz6482/map510_fit.mov?rlkey=ekz3aw63bot5435tqkd8qnz5z&dl=0

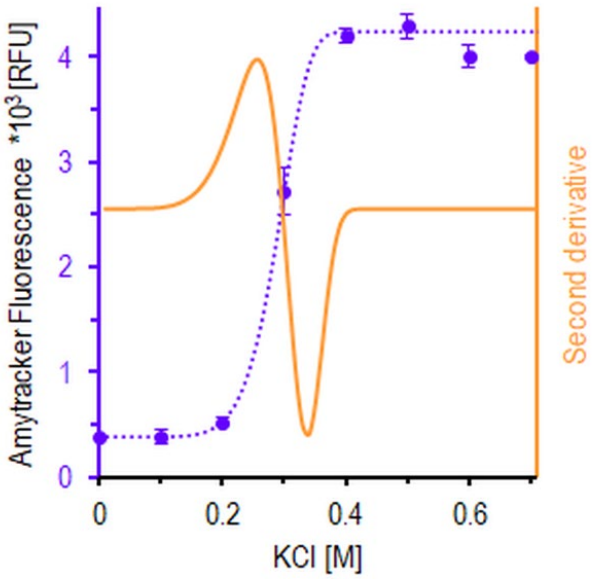

Figure S1. Effect of salt concentration on PFK-Amytracker fluorescence. Raw data (purple) the fitted line for sigmoidal increase (purple, dotted). The second derivative of the fitted equation appears in continuous line (orange). The calculated critical KCl concentration was calculated as the intercept of the second derivative curve with concentration axis (x-axis) to be 327 mM per 0.2 mM concentration of PFK. The contribution of PFK and the buffer to the ionic strength is negligible, with effective ionic strength of 0.3 M due to the high KCl concentration.

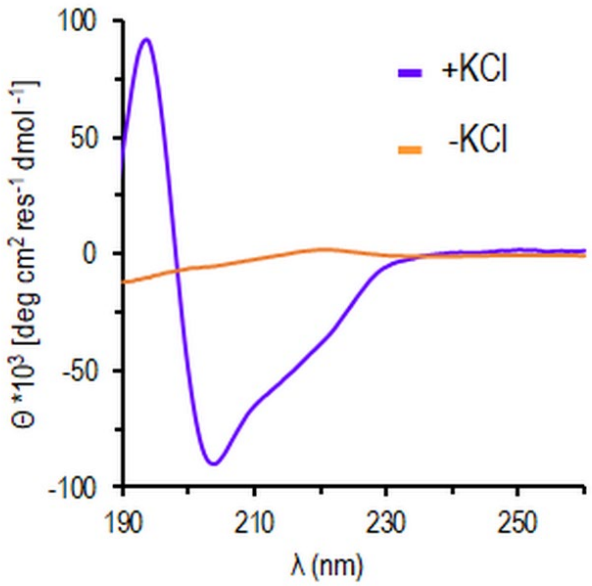

Figure S2. Circular dichroism (CD) spectroscopy of PFK. PFK monomers were dissolved in 5 mM Hepes buffer (pH 7.4) with and without added KCl (0.3 M). 40 µL of the PFK samples, in concentration of 0.2 mM, were placed in quartz cuvette (pathlength of 0.01 cm) and the CD spectra were obtained using a Jasco J-715 spectropolarimeter (Tokyo, Japan) within the range of 185–260 nm. Samples were prepared in a diluted Hepes buffer (5 mM) to minimize buffer-dependent noise. Spectra were recorded at a wavelength data pitch of 0.5 nm at temperature of 20 °C, representing an average of four scans. Buffer background was recorded and subtracted from the corresponding spectra. The ellipticity (θ) was normalized based on path length, peptide concentration, and number of residues, presented as mean residual ellipticity (θ_{MRE}).

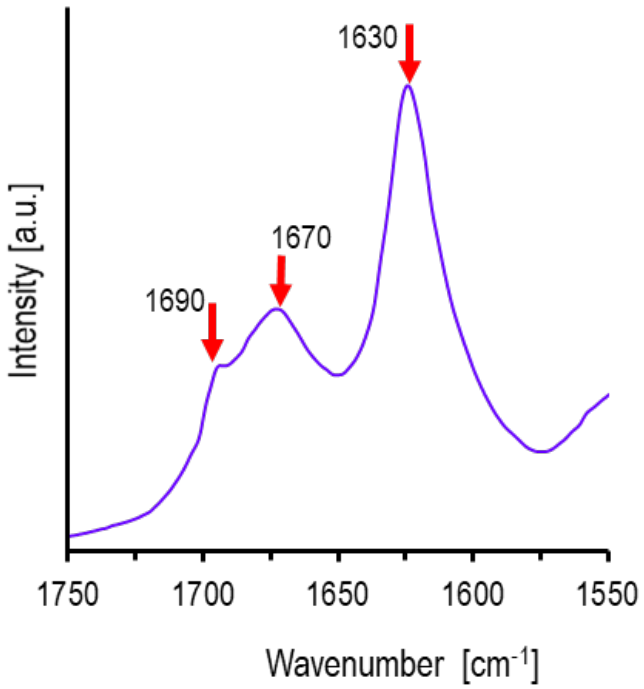

Figure S3. Fourier transform infrared spectroscopy (FTIR) of PFK. Peptide samples were prepared by incubation of 0.2mM PFK in 10mM ammonium acetate buffer having 0.2M KCl, utilizing an ammonium acetate buffer (10 mM, pH = 7.35). After incubation, the samples were transferred to plastic test tubes and rapidly frozen using liquid nitrogen. Subsequently, the samples underwent lyophilization at -30°C to maintain their secondary structure integrity (performed using LABCONCO-Triad, Labotal, Israel). FTIR spectra were monitored using a NICOLET 6700 FTIR spectrometer equipped with an attenuated total reflectance (ATR) system featuring a diamond crystal and a DTGS detector (Thermo Fisher Scientific, MA, USA). Spectra acquisition involved 188 scans at a resolution of 4 cm-1 and was corrected for any spectral distortions using atmospheric suppression techniques. Baseline correction was applied uniformly across all spectra. Reference spectra were obtained using a bare ATR crystal surface. Marked with red arrow 1670-1690 antiparallel beta-sheet structure and 1620-1630 beta-sheet structure.

a

Step	Time, min	MP A, %	MP B, %
1	Initial	90.0	10.0
2	5.00	40.0	60.0
3	7.50	40.0	60.0
4	10.00	10.0	90.0
5	11.00	10.0	90.0

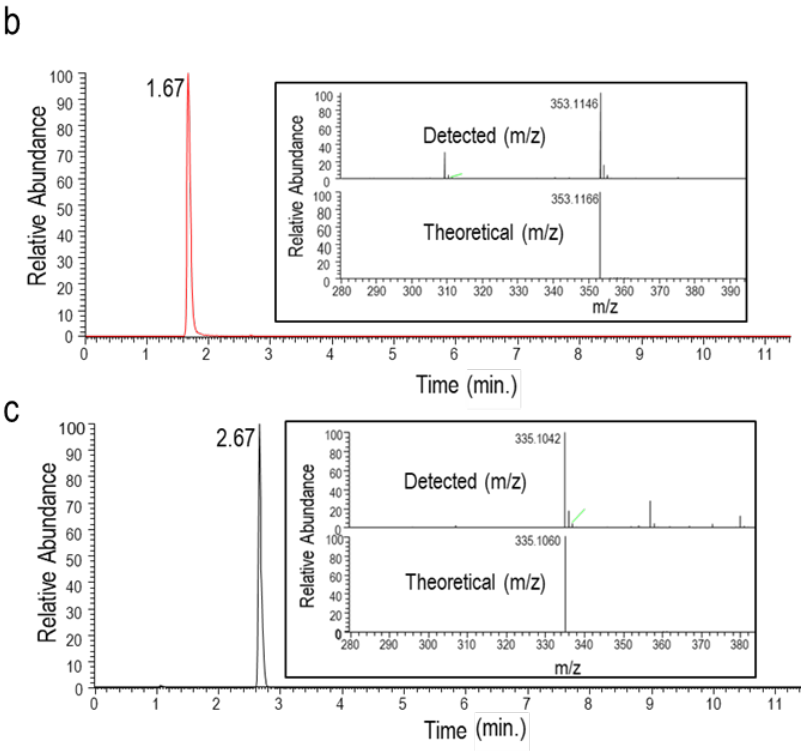

Figure S4. Catalytic degradation of Penicillin: LC-MS analysis. a. LC Gradient protocol for Penicillin. **b.** LC-MS chromatogram of *degraded-Penicillin*. In the inset, mass spectra of Penicillin and the theoretical calculated value. The smaller peak 310 m/z represent penilloic acid). **c.** LC-MS chromatogram of *fresh* Penicillin. In the inset, mass spectra of the penicillin. The column temperature was maintained at 40°C, while the sample temperature remained at 10°C. A constant flow rate of 0.4 mL/min. was employed throughout the experiment, with a total runtime of 11 minutes. Mobile phase (MP) A consisted of water with 0.1% formic acid, MP B comprised of acetonitrile. The solvents (water, formic acid, acetonitrile) were used in LCMS-grade. The experiments were conducted in triplicate, and the results presented here are representative of those three independent trials.

a

Step	Time, min	MP A, %	MP B, %
1	Initial	90.0	10.0
2	3.00	40.0	60.0
3	4.50	40.0	60.0
4	6.00	10.0	90.0
5	7.00	10.0	90.0

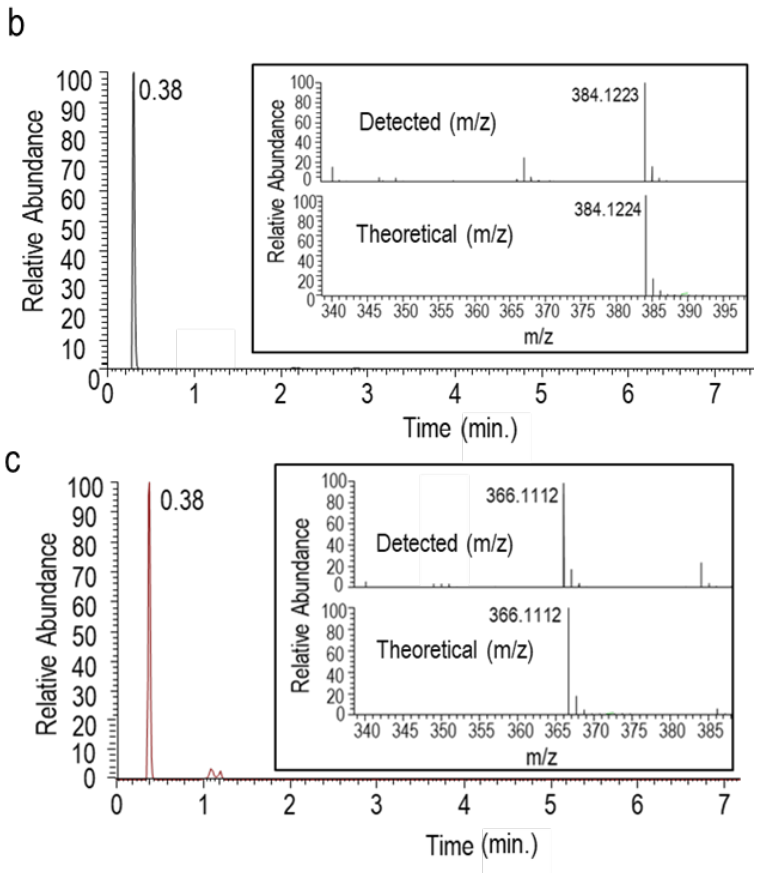

Figure S5. Catalytic degradation of Amoxicillin: LC-MS analysis. a. LC Gradient protocol for amoxicillin. **b.** LC-MS chromatogram of *degraded*-amoxicillin. In the inset, mass spectra of amoxicillin and the theoretical calculated value. **c.** LC-MS chromatogram of *fresh* amoxicillin. In the inset, mass spectra of the degraded amoxicillin. The column temperature was maintained at 40°C, while the sample temperature remained at 10°C. A constant flow rate of 0.4 mL/min was employed throughout the experiment, with a total runtime of 7 minutes. Mobile phase (MP) A consisted of water with 0.1% formic acid, MP B comprised of acetonitrile. The solvents (water, formic acid, acetonitrile) were used in LCMS-grade. The experiments were conducted in triplicate, and the results presented here are representative of those three independent trials.

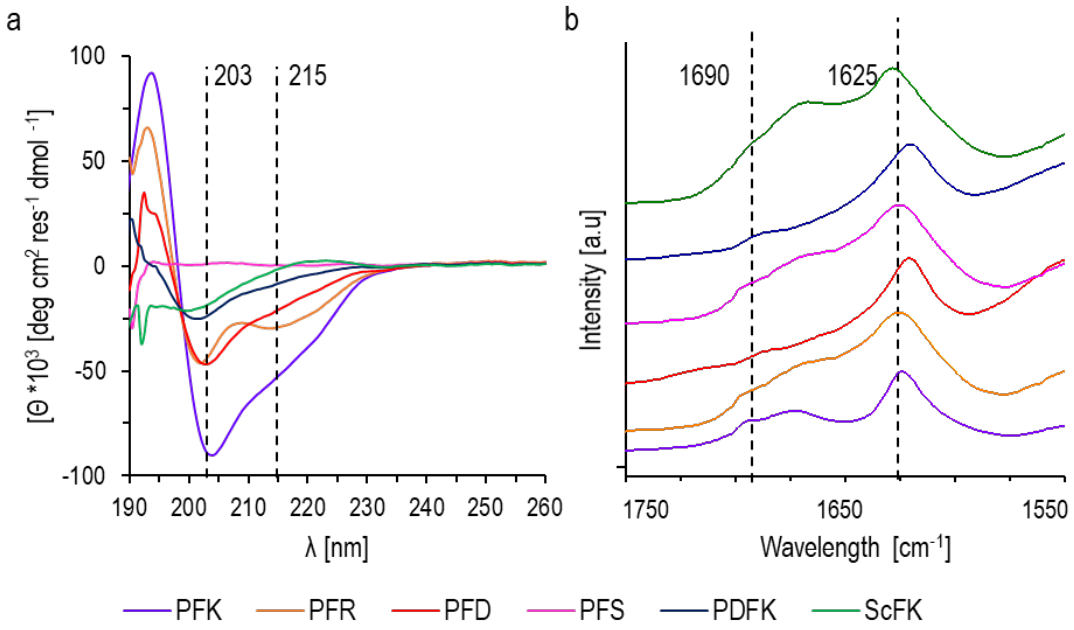

Figure S6 Secondary structure analysis of PFK homologous. a. Circular Dichroism (CD) spectroscopy; **b.** Fourier transform infrared (FTIR) spectroscopy. The samples for CD analysis were prepared as reported as mentioned above (Figure S3). For FTIR analysis, the samples were prepared similarly using ammonium acetate buffer (5 mM, pH 7.4) andincubated for 2h. Ammonium-acetate buffer was used due to its ability to partially evaporate along the lyophilization, allowing smaller buffer fingerprint and noise. Following the incubation, the samples were cryogenically snap-frozen by dipping in liquid nitrogen. Following this, the samples were lyophilized at -30˚C to preserve the secondary structure (LABCONCO-Triad, Labotal, Israel). FTIR spectra were recorded using NICOLET 6700 FTIR spectrometer with attenuated total reflectance (ATR) system equipped with diamond crystal and DTGS detector (Thermo Fischer Scientific, MA, USA). The FTIR spectra were acquired from xxx scans at 4 cm^{-1} resolution and were corrected for spectral distortion using atmospheric suppression. A baseline correction function was applied to all spectra. Reference spectra were measured using bare ATR crystal surface.

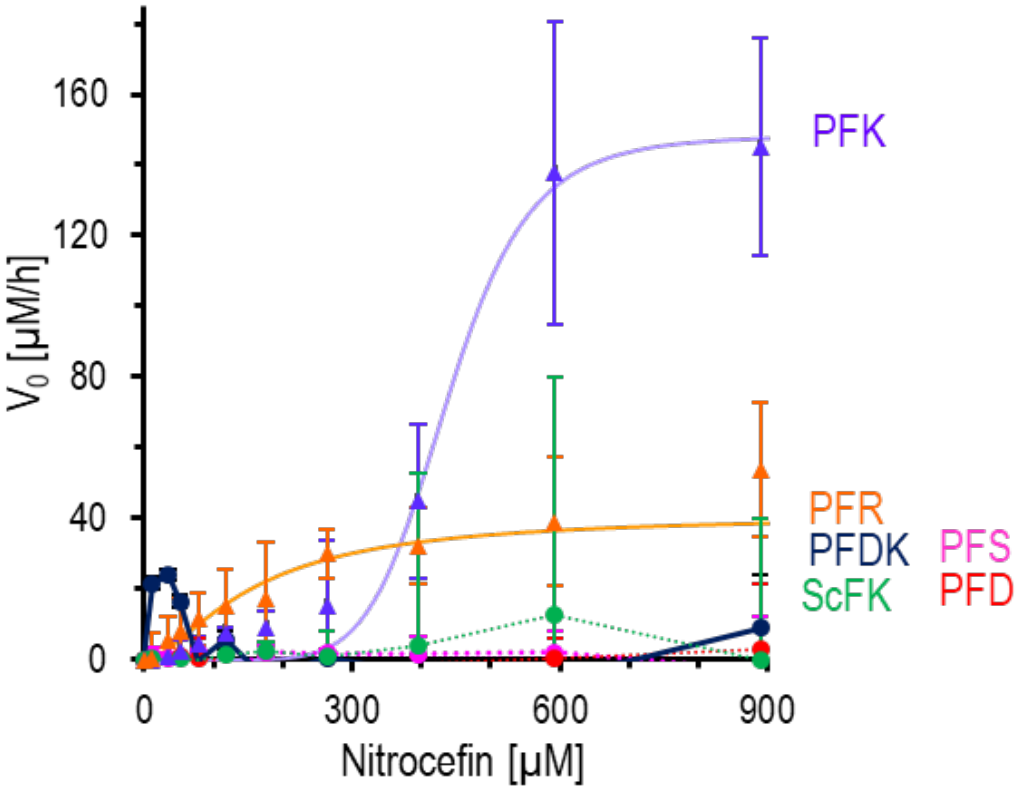

Figure S7. Initial rate vs concentration of nitrocefin hydrolysis by PFK homologues. The peptide concentration in all samples was 0.2 mM, dissolved in Hepes 50 mM pH 7.4, KCl 0.2 M. The values are presented as an average±SEM, n=5.

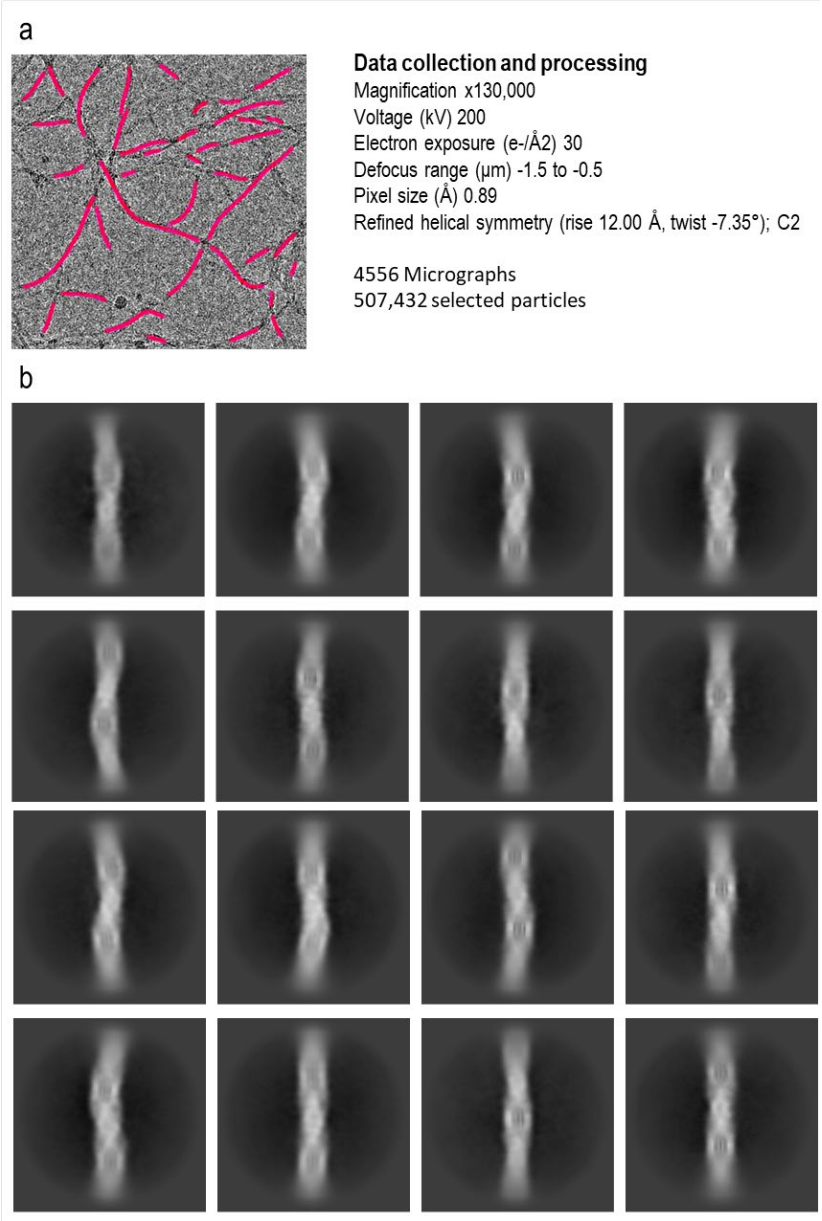

Figure S8. Single particle analysis of cryo-EM images: Filament sample processing. PFK-nitrocefin samples were prepared as described above at PFK concentration of 0.2mM and nitrocefin concentration of 0.7mM. The samples were mixed, deposited on EM-grid, snap-frozen and imaged as described above. **a.** Representative cryo-EM micrograph with particles picked using

Filament tracer in CryoSPARC. **b.** Two-dimensional class averages selected for further processing (out of 50).

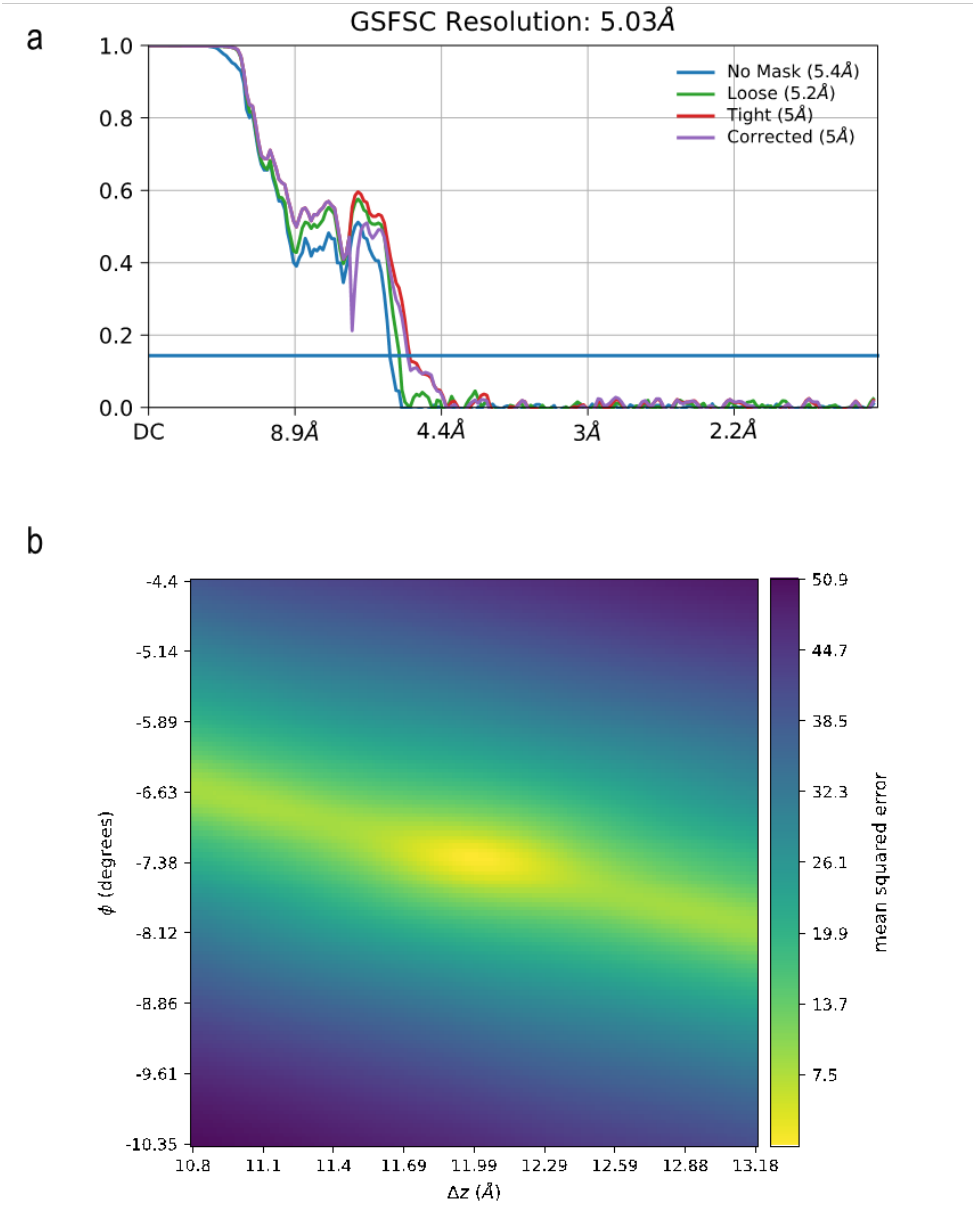

Figure S9. Filament analysis. a. Fourier Shell Coefficient (FSC) plot measured by the Gold-standard method. **b.** Helical Symmetry Error Surface plot showing minima at a rise of 12.00 Å and a twist at -7.35°.

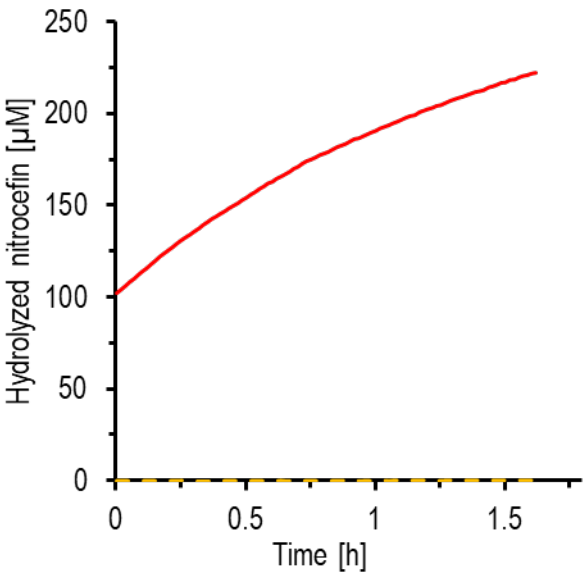

Figure S10. Catalytic activity of PFK$_{DOPA}$ towards nitrocefin degradation. PFK$_{DOPA}$ fibrils samples were prepared as described above, at peptide concentration of 0.2Mm(dissolved in Hepes 50 mM, pH 7.4, KCl 0.6 M). The samples were mixed with fresh nitrocefin (0.67 mM) and 50 µL of the samples was transferred to 96 well plate, and the absorbance was measured every 1 minutes for two hours (Biotek synergy, MA, USA).

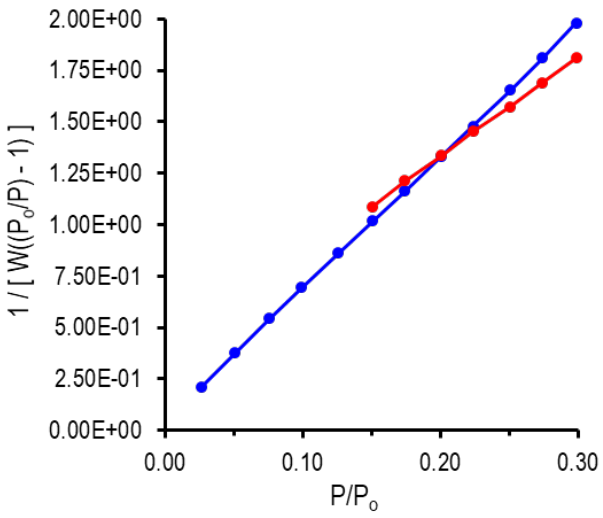

	Coated beads	Uncoated beads
Slope (g^{-1})	4.801	6.420
Intercept (g^{-1})	3.763e-01	4.961e-02
Correlation coefficient, r	0.999967	0.999925
C constant	13.759	130.405
Surface Area (m^2/g)	672.694	538.30

Figure S11. Brunauer-Emmett-Teller (BET) analysis of bare and PFK-coated silica beads. Coated silica beads [10µm dimeter] were prepared described above. Bare and coated beads were lyophilized and 100µg of beads surface area was analyzed using BET analysis.

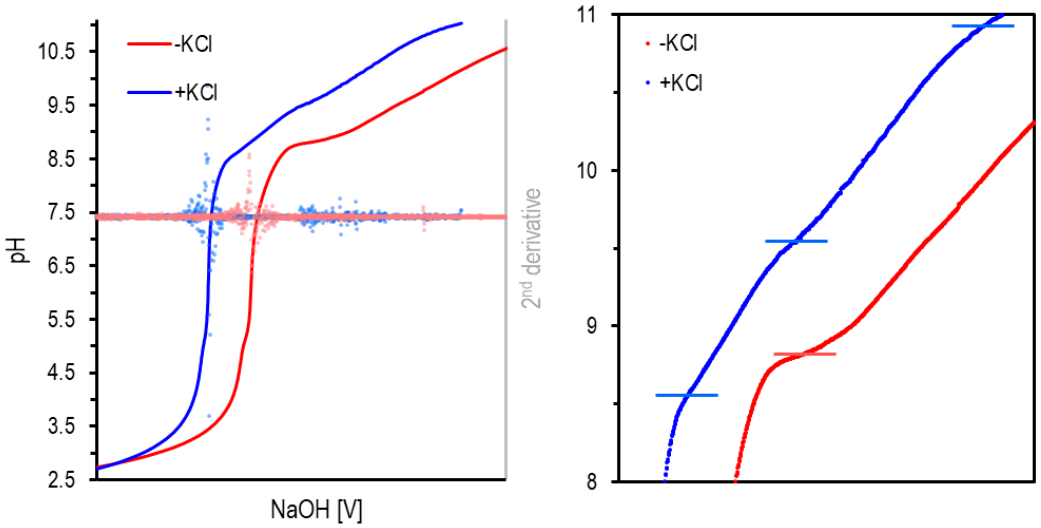

Figure S12. pH titration of PFK. Titration from acidic to basic pH of 1 mM PFK with or without KCl 0.3 M (blue and red, respectively). On the left – the full curve, and on the right – magnified area of the pH curves, the horizontal lines represent the short plateau areas in which the sample is buffered. The continuous line is the titration pH curve upon gradual addition of 1 µL NaOH 0.05 M drops in rate of one drop per three seconds.

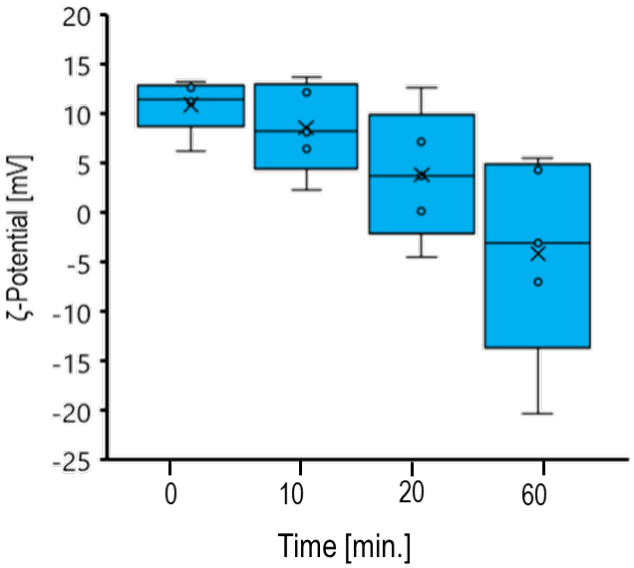

Figure S13. The ζ-potential of PFK fibrils upon coincubation with nitrocefin: Kinetic measurement. The ζ-potential was measured using a Zetasizer (Zetasizer Nano ZS, Malvern,

Worcestershire, UK) using Malvern DTS 1070 disposable U-shape capillary cuvettes. 1 mL of PFK sample, containing preformed fibrils in concentration of 0.2 mM were prepared as described above (Hepes 50 mM pH 7.4, KCl 0.2 M). The fibrils were then mixed with nitrocefin, in concentration of 0.6M, and the ζ-potential was measured at time points of 0, 10 20 and 60 minutes. The values are presented as an average±SEM, n=5.